Geophys. J. Int. (2002) **148,** 256–277

Morphological dating of cumulative reverse fault scarps: examples from the Gurvan Bogd fault system, Mongolia

S. Carretier,[1,*] J-F Ritz,[1] J. Jackson[2] and A. Bayasgalan[2]

[1] *Laboratoire de Géophysique Tectonique et Sédimentologie, CNRS-UMR, Université Montpellier II, 4, Place Eugène Bataillon, 34000 Montpellier, France. E-mail: scarret@dstu.univ-montp2.fr*

[2] *Bullard Laboratories, Madingley Road, Cambridge, CB3 OEZ England*

Accepted 2001 September 20. Received 2001 July 3; in original form 2000 August 10

SUMMARY

We relate reverse fault scarp morphology formed by several earthquake dislocations to the average deformation rate, using a morphological dating model based on a diffusion analogue of erosion. Our scarp degradation model includes diffusive erosion during the interseismic period, the gravitational collapse of the coseismic fault scarp just after formation, and the variation of the surface rupture location. Interactions between thrusting and geomorphic processes acting on scarp morphology are analysed along the Gurvan Bogd Range in Mongolia. Four main processes acting on scarp morphology were distinguished: 1) gravitational collapse of the frontal scarp, resetting the diffusive scarp if fault offsets are big and faulting is localized; 2) progressive erosion of the fault scarp during the interseismic period; 3) folding associated with the frontal thrust and backthrusts; 4) competing alluvial deposition on mountain piedmont slopes and abrasion of the fault scarp by wash processes. The growth of cumulative reverse fault scarps is suppressed when they are located in the outwash of major drainage basins. They can grow higher in distance from major catchment discharges. The modelling suggests that the morphology of the scarp and its apparent degradation stage, depend on the parameters controlling the amount of frontal collapse; the magnitude of coseismic offsets, the dip of the fault near the surface and the step distance between faults. Folding associated with thrusting creates a convexity on the upper part of the scarp and increases its height. The comparison of different scarp profiles suggests that folding leads to an overestimate of the morphological age. We estimate a diffusion coefficient at 3.3 ± 1.7 m^2 ka^{-1}. Morphological ages calculated with our model confirm that slip rate along reverse faults of the Gurvan Bogd range has not been constant over the last 100 ka.

Key words: cumulative fault scarp, earthquake, erosion, morphological dating, reverse faulting, uplift rate.

1 INTRODUCTION

Dating geomorphic features is one of the main problems in quantitative geomorphology, especially applied to active tectonics. In addition to the recent development of numerical dating methods (e.g. surface exposure dating using cosmonucleides—e.g. Brown *et al.* 1991; Bierman *et al.* 1995; Ritz *et al.* 1995; Siame *et al.* 1997; Bourlès 1992), numerical modelling of landscape evolution has opened the way to what is called morphological dating (e.g. Culling 1960; Hirano 1968; Bucknam & Anderson 1978; Nash 1984; Hanks 1999). This approach is useful in studies of active tectonics because it allows us to characterize the degradation of a marker according to the rates of vertical movement and erosion. Morphological dating has been applied mainly in the cases of one-event fault scarps, terrace risers (e.g. Nash 1984; Hanks & Schwartz 1987; Enzel *et al.* 1996) and cumulative normal fault scarps (Avouac & Peltzer 1993; Nash 1981). In this paper, we are concerned with estimating slip rates from morphological dating of cumulative reverse fault scarps found in the Gurvan Bogd fault system in Mongolia.

The Gurvan Bogd range forms the eastern terminus of the Gobi Altay mountain range of Mongolia (Fig. 1), and is composed of three massifs (Ih Bogd, Baga Bogd, Artz Bogd) corresponding to transpressional segments of a left-lateral strike-slip system that is 600 km long. Active reverse faults along the Gurvan Bogd range cut through alluvial fans and terraces on the piedmont slope of the mountains. This is a general feature which is also observed in other places in Central Asia, for example in Southern Tibet and the

*Now at: BRGM, dept. ARN, 3 ave Claude Guillemin, BP6009, 45060 Orleans, France. E-mail: s.carretier@brgm.fr

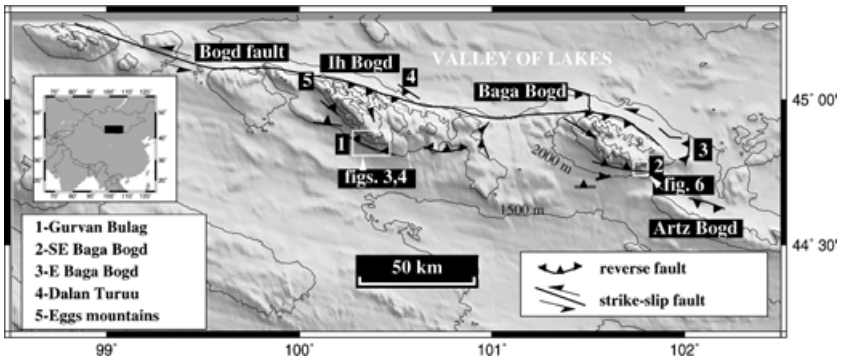

Figure 1. The Gurvan Bogd Range in the eastern Gobi Altai of Mongolia, showing our study locations.

Tien Shan (Tapponnier & Molnar 1979; Armijo *et al.* 1989; Avouac *et al.* 1993; Molnar *et al.* 1994). Such reverse fault scarps located away from the main rangefront have been called "forebergs" (e.g. Bayasgalan *et al.* 1999a).

The 1957 December 4 Gobi Altay earthquake (magnitude 8.3) led to a 260 km left-lateral surface rupture and 100 km of surface rupture by reverse faulting along the Gurvan Bogd range (Kurushin *et al.* 1997). This earthquake was the focus of seismotectonic studies (e.g. Florensov & Solonenko 1963; Baljinnyam *et al.* 1993; Bayarsayhan *et al.* 1996; Schwartz *et al.* 1996; Kurushin *et al.* 1997; Bayasgalan 1999; Bayasgalan *et al.* 1999a). Recent works (Bayasgalan *et al.* 1999a,b) investigated the relationships between the strike-slip faults and thrust faults in this region. Both are involved in rotations of crustal blocks about vertical axes, accommodating SSW–NNE shortening due to the India–Eurasia collision. In this context, the thrust faults are directly involved in the recent uplift of the Gurvan Bogd mountains (Bayasgalan *et al.* 1999a,b; Owen *et al.* 1999). Other studies were concerned with the climate-related alluvial fans cut by the faults along the Gurvan Bogd range (Ritz *et al.* 1995; Owen *et al.* 1997; Carretier *et al.* 1998), and with the geomorphic evolution of forebergs (Bayasgalan *et al.* 1999a). Bayasgalan *et al.* (1999a) observed a wide range of reverse fault scarp morphologies depending on their stages in development and their alluvial environments. The evolution of thrust scarps into topographic ridges seems to be related to fault geometry and the development of backthrusts and folding (Bayasgalan *et al.* 1999a). In addition Owen *et al.* (1998, 1999) used arguments based on soil development and the dating of Quaternary sediments to propose that the formation of alluvial fans at the foot of the Gurvan Bogd range is mainly controlled by climatic variations. They identified the following succession: 1) sedimentation under humid conditions dominated by perennial streams; 2) an increase in aridity causing a coating of coarse fanglomerates over the precedent fans by ephemeral streams and the development of permafrost (22–15 ka); 3) the degradation of the permafrost and fan incision during early Holocene (13–10 ka). According to Owen *et al.* (1999), deformation of fans by thrusting is contemporary with this last stage. Ritz *et al.* (1999) dated several alluvial surfaces along the Gurvan Bulag fault using cosmucleides (Fig. 1). Their datings suggest that two major periods of alluviation occurred at 118.6 ± 17.8 ka and at 12.7 ± 1.95 ka. The offsets of these alluvial surfaces lead to uplift rates at 0.18 ± 0.05 mm yr^{-1} over the last 118.6 ± 17.8 ka, and 1.37 ± 0.25 mm yr^{-1} over the last 12.7 ± 1.95 ka. According to Ritz *et al.* (1999), the Gurvan Bulag reverse fault evolved from a quiescent fault to a fault generating strong dislocations ($\sim$4 m), separated by an interval of a few thousands of years (3.3 ± 1 ka). This interval is consistent with results of palaeoseismological investigations (Bayasgalan *et al.* 1997). This example of variation of fault activity in time motivated us to study the vertical slip rates in this particular area. Therefore, the fault scarps observed at the front of the Gurvan Bogd Range are particularly suitable for estimating deformation rate from morphology because they are well preserved. Indeed, the aridity, the lack of vegetation, the absence of human activity and the size of coseismic fault displacements (between 1 to 5 m of vertical offset along the Gurvan Bulag thrust fault during a single earthquake in 1957, Fig. 1) allow an unspoilt development of geomorphic markers that is not common elsewhere.

Only few studies have tackled the problem of morphological dating of cumulative reverse faults (Hanks *et al.* 1984, 1997; Arrowsmith *et al.* 1996). Because the interactions between faulting history and erosion can be complex in such tectonic context, it is necessary to identify from field observations the different processes controlling the reverse faults scarps morphology. In this paper, we first analyse the geomorphic relationships between alluvial sedimentation, erosion and faulting for some of the thrust fault scarps along the Gurvan Bogd range. This qualitative analysis is based on descriptions of aerial photographs, precise GPS levelling of scarp profiles and field observations. Then, we apply a simple scarp degradation model to several scarp profiles to estimate the morphological age of the deformation. This approach allows us to identify the dominant geomorphic processes and to test the limitation of our model in each case. Finally, we compare our results with previous results concerning the seismic activity along the Gurvan Bogd range.

2 GEOMORPHIC ANALYSIS OF THE STUDIED THRUSTS ALONG THE GURVAN BOGD RANGE

In this section, the geomorphological evolution of reverse fault scarp is considered by analysing the interactions between fan formation and thrusting for two reverse faults of the Gurvan Bogd range.

2.1 The Gurvan Bulag fault (Figs 1 and 3)

The Gurvan Bulag reverse fault scarp is 23 km long, with an E-W strike, and is roughly 5 km south of the foothills of Ih Bogd massif (Figs 1, 2a,c). The 1957 December 4 earthquake ruptured the entire length of the Gurvan Bulag scarp, producing 3–5 m high vertical offsets (Kurushin *et al.* 1997). Along the Gurvan Bulag fault (Fig. 1), deformed zones by reverse faulting can vary even over a few kilometres as illustrated by Fig. 3. This figure shows spot images of alluvial fans cut by the Gurvan Bulag reverse fault. In regions A and C of Fig. 3 the fault scarp has reached a height of 100 m, associated with the development of a ridge. In region B in the front of a main drainage basin outlet, the fault scarp is less developed. The

Figure 2. Field photos. Triangles point the thrusts location. (a) View N of the Gurvan Bulag thrust, in front of a drainage basin outlet on the southern side of Ih Bogd (site 1 on Fig. 1). (b) Preserved ridge of the Dalan Turuu Forberg on the northern side of Ih Bogd (site 4 on Fig. 1), view S. (c) View E of the Gurvan Bulag cumulative thrust scarp (∼20 m high) (site 1 on Fig. 1). Note the frontal location of the 1957 scarp. (d) Trench across the N-S cumulative thrust scarp at eastern end of Baga Bogd (site 3 on Fig. 1), view SW. The faulting has remained localized at each event on a 45°-dipping fault cutting the surface at the inflection point of the scarp profile (triangle). Dotted lines underline the undeformed stratification, showing that the scarp morphology is controlled by slope erosion and not by bending. E) View E of the cumulative thrust scarp (∼20 m high) located SE of Baga Bogd (site 2 on Fig. 1). (f) Example of a cumulative reverse fault scarp morphology mainly controlled by internal structure (Eggs mountains, site 5 on Fig. 1). (g) Example of cumulative reverse fault scarp (∼ 20 m) along the Gurvan Bulag foreberg, the form of which is mainly controlled by gravitational processes. At this place, frontal collapse has reset most of the diffusive scarp from 1957 earthquake.

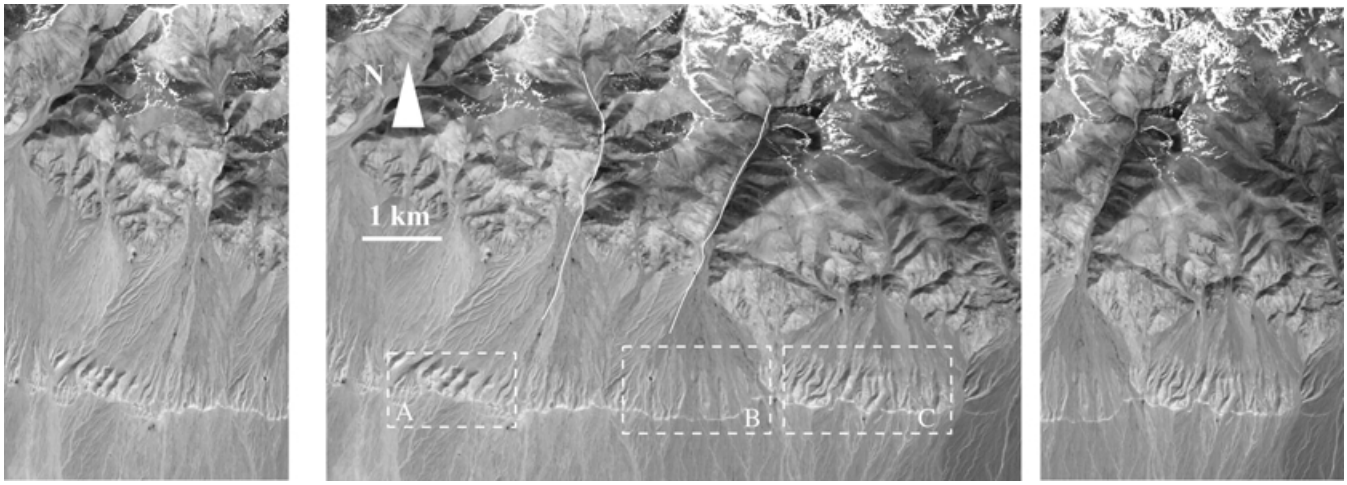

Figure 3. Stereo Spot images of the Gurvan Bulag thrust scarp (see Fig. 1 for location). This figure illustrates the differences in scarp morphology along the thrust scarp. White lines underline the active streams flowing from the two main drainage basins. Dotted frames demarcates three regions where cumulative scarps look clearly different. In frames A and C, away from the main drainage outlets, the thrust scarps correspond to well developed ridges ∼100 m high associated with folding and backthrusting (Bayasgalan *et al.* 1999a). In frame B, in front of a main drainage outlet, the deformed alluvial fans look more linear, without well developed ridge.

topographic ridges developed in regions A and C, are associated with pure reverse movement on the thrust and en échelon fractures and backthrusts which accommodate a strike-slip component (Bayasgalan *et al.* 1999a).

We used aerial photographs to identify four uplifted alluvial surfaces (s1 to s4, Fig. 4). We based our analysis on the density of drainage networks and relative heights of terraces to give relative ages to the different surfaces (e.g. Bull & Pearthree 1988; Siame *et al.* 1997). The oldest surface (s1) is incised by dendritic drainage networks. Where natural incision reveals a cross-section, it appears that this surface corresponds to alluvial deposits in which granite boulders typically 0.1–1.0 m in diameter can be found. These deposits are deformed along the scarp, leading to a deeply incised ridge, 500 m to 1 km wide and parallel to the thrust. In the central part of the Gurvan Bulag foreberg (Fig. 4) a large part of surface s1 has disappeared, removed by the two main outwash channels.

The second surface (s2) is also incised by dentritic drainage networks. It cuts into the surface s1 starting at the apex of the fans and forms terraces along the fault scarp. This s2 surface is mainly visible within the central part of the region, in front of major outwash systems (Fig. 4). This suggests a period of degradation after the deposition of s1, followed by the deposition of s2. The vertical offset of this s2 surface along the scarp is 17–20 m high. The age of this surface has been estimated from cosmogenic dating at 118.6 ± 17.8 ka (Ritz *et al.* 1999). Some relics of the s2 surface (s2b) are sometimes difficult to differentiate from a younger surface s3 (Fig. 4).

The s3 surface corresponds to debris flows. Its morphology is characterized by bars and swales, and rill-wash features. It covers a large part of the older fan surfaces north of the foreberg, which provided a barrier to the sedimentation (Bayasgalan *et al.* 1999a). The thin coating of this deposit, made of coarse boulders typically 0.1–1.0 m in size, hampers its cartography. Consequently, some portions of surface s3 that we reported on Fig. 4 may correspond to eroded older deposits (in particular s2b). Ritz *et al.* (1999) dated surface s3 at 12.7 ± 1.95 ka. This age is consistent with an estimated age of permafrost relics located around Artz Bogd (Fig. 1), which Owen *et al.* (1998) suggest corresponds to a Holocene transition from an arid and cold period to a warmer period.

The s4 surface corresponds to terraces inset in surface s3. Its vertical offset along the fault is ∼6.5 m. The fact that it is located along the scarp suggests a tectonic origin. Ritz *et al.* (1999) dated this surface at 4.1 ± 0.7 ka.

We levelled topographic profiles across these different uplifted surfaces using differential GPS (Fig. 5). The repeatability in altitude is the order of centimetres. This is an acceptable precision to compare the profiles, considering that the scarp offsets exceed several metres.

The gravity-controlled failure associated with the 1957 December 4 event affected the fault scarp differently from place to place. On the profile P5 (Fig. 5), most of the scarp slope has been reset by gravity-driven processes since the 1957 event. Consequently, if we measure the 1957 offset from the vertical height of the gravity-controlled face on the profile P5, we overestimate it (Fig. 5). On other profiles (e.g. P6 and P2, Fig. 5) the 1957 offset is localized at the base of the cumulative fault scarp, that allows the rest of the scarp to be preserved from collapse. The preserved smooth morphology on scarp profiles P1, P2, P3 and P6 (Fig. 5) corresponds to the previous surface ruptures eroded by slope erosion. This suggests that faulting steps forward in each event.

Scarp profiles P2 and P6 (Fig. 5) show constant slopes, whereas profile P1 levelled between regions A and B (Figs 3, 4 and 5) shows a convexity behind the frontal scarp. This convexity forms a ridge and drainage barrier at the western and eastern ends of the Gurvan Bulag foreberg. Where does this convexity come from and what controls its amplitude? Bayasgalan *et al.* (1999a) pointed out the occurrence of both thrusts and backthrusts along the Gurvan Bulag fault scarp. Although our profiles are not exactly at the same places as Bayasgalan *et al.*'s observations, we interpret the convexity shown on profile P1, as morphological consequences of folding and backthrusting. This convexity is located between $x \sim 550$ m and $x \sim 800$ m on profile P1 (Fig. 5). The fault scarp is located near $x \sim 480$ m. Between the fault scarp ($x \sim 480$ m) and the beginning of the convexity, the slope corresponds to the undeformed alluvial slope (Fig. 5). Consequently, it seems that the folding in this case is associated more with backthrusting than with the main thrust. Profiles P3 and P4 have been levelled across less uplifted zones (Figs 4 and 5). No clear folding appears on topography at this place.

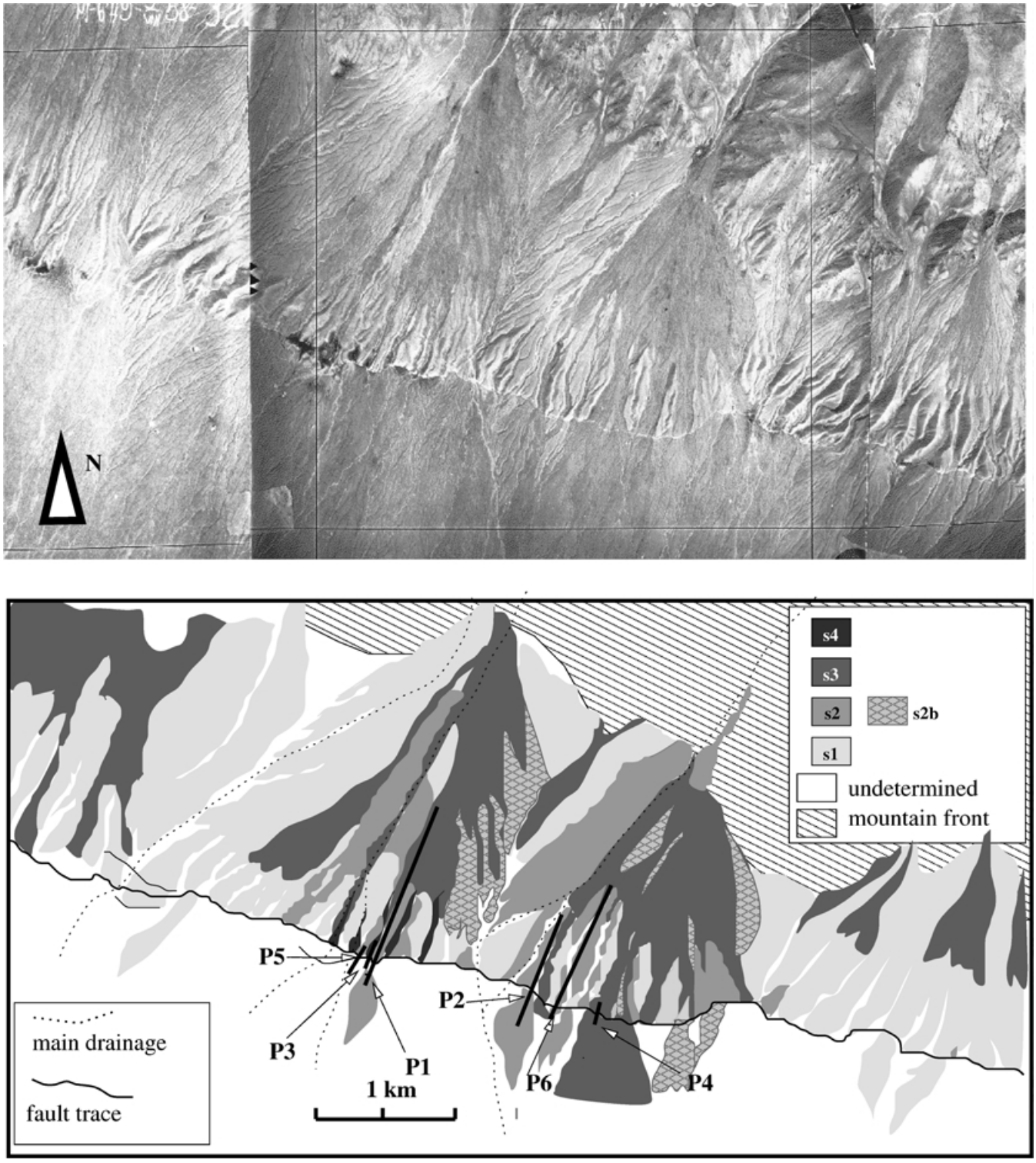

Figure 4. Geomorphic analysis of aerial photos along the Gurvan Bulag foreberg, showing the locations of profiles used in Fig. 5. We identified several alluvial surfaces from their relative elevation, and field observations. Surface s1 is the older and the more uplifted surface. Surface s2 corresponds to an alluvial fan incased in s1. We interpret s2b as relics of surface s2 partially covered or washed by posterior alluvial deposits. Surface s3 corresponds to a thin alluvial deposits incased of covering at some places s2. Surface s4 is the youngest surface, and it is located near the fault. Thick black lines indicate the location of topographic profiles shown on Fig. 5. Solid lines show the location of scarp profiles (P1 to P6). These profiles were levelled in portions of scarp not altered by runoff driven processes.

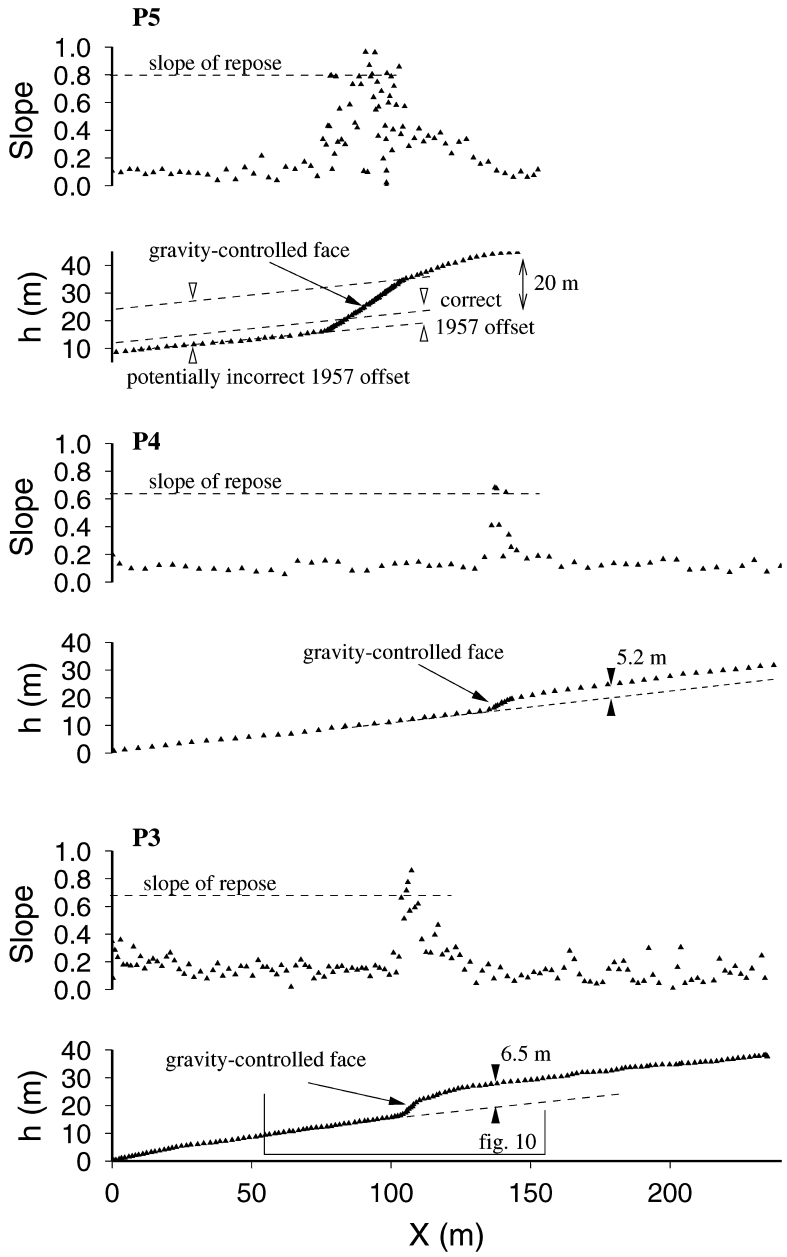

Figure 5. Elevation and slope profiles levelled across the Gurvan Bulag thrust (see Fig. 4 for localization). Note that on profile P5 the vertical height of the gravity-controlled face greatly exceeds the value of the 1957 offset known at this place. Note also that on profile P1 the surface s3 stops at the onset of the convexity that we interpret as a surficial effect of folding and backthrusting. On the contrary, profiles P2 and P6 show constant regional slope upwards from the top of the scarp.

This suggests that folding grows in amplitude with the number of events and when backthrusting has taken place. However, we do not have any trench evidence that no folding occurred at this place in relation with the main thrust. In some other places along the Gurvan Bogd range, trenches show a simple reverse fault cutting through undeformed sediments (for example, see Fig. 2d). Other examples show that a part of the fault scarp is controlled by bending (for example, see Fig. 2f). Consequently, folding is not a general feature in this area. When it develops, it can cause the scarp to appear older, because it gives an apparent eroded shape upwards (Fig. 2f). This should strongly limit the morphological dating of such scarps. We will evaluate this effect from the analysis of scarp profiles in a next Section. The other main controls on the amplitude of the convex ridge are drainage and sedimentation. On one hand, the convex ridge developed in the oldest surface s1 disappears in the central part of Gurvan Bulag, in the front of the two main drainage basins, which have presumably eroded it away during periods of high fluvial transport (see frame B of Fig. 3). On the other hand, where the ridge acts as a barrier, sedimentation which accumulates behind it also tends to level the convexity. By successive alluvial filling, the convexity tends to disappear by burial. On the profile P1 (Fig. 5), the alluvial fan s3 stops against the convexity developed in s2. This effect explains why profiles P2 and P6 look roughly linear (Fig. 5). The area in front of the main drainage basins is also one of abundant alluvial supply. Despite the linear fan shape observed on profiles P2 and P6 levelled on the surface s2, this surface is

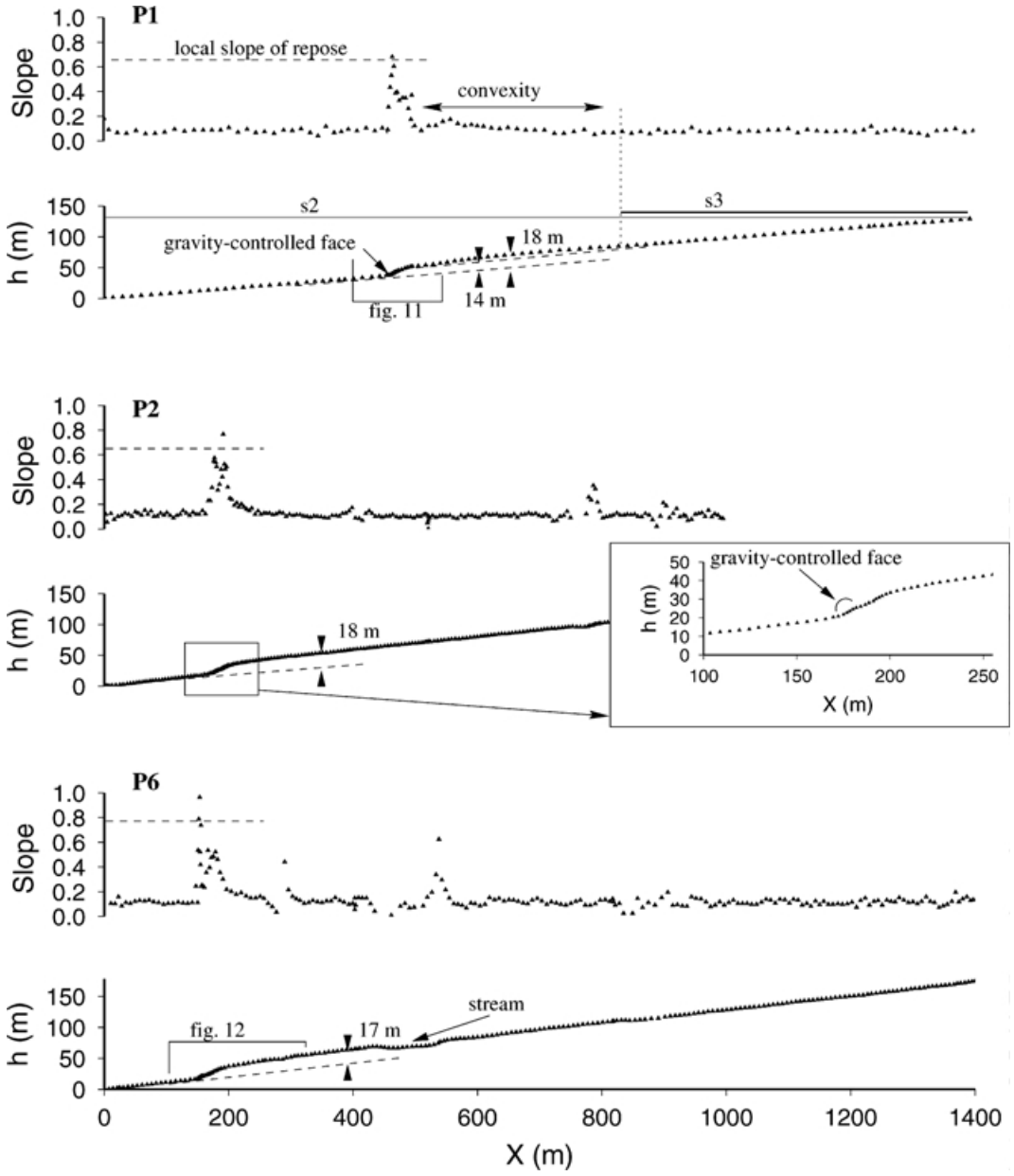

Figure 5. (*Continued.*)

probably not all of one age between the fan apex and the fault scarp (Fig. 4).

2.2 E–W thrust scarp to the south of Baga Bogd (Figs 1 and 6)

We identified four geomorphic surfaces at this place (s1, s1b, s2, s3) (Fig. 6). These surfaces were not cut by thrusting in the 1957 earthquake (Florensov & Solonenko 1963). The oldest one (s1) is incised by dendritic drainage networks and is the highest recognizable surface uplifted by the reverse fault. Natural incision reveals that this surface corresponds to alluvial deposits in which granite boulders typically 0.1–1.0 m in diameter can be found. The second surface (s1b), uplifted ∼15 m by the thrust, is embedded in s1. We interpret s1b as a wash surface, probably corresponding to a humid pulse during the early history of the uplift. The third surface (s2) has an intermediate character between dendritic incision and bar-and-swales. The presence of this surface within the apex of s1 suggests that it formed during an aggradation period and is thus a fan surface (Fig. 6). Surface s2 is also affected by the thrust. The most recent surface (s3) has a bar-and-swales character and corresponds also to an alluvial surface. This surface has not been uplifted (Fig. 6). Consequently, the thrusting activity on this scarp occurred before the deposition of s3 and stopped between the depositions of s2 and s3. However, we do not have dating information for these surfaces. So, although surface s3 at this location has the same geomorphic features as surface s3 at the Gurvan Bulag fault (dated at 12.7 ± 1.95 ka), we can not prove that these surfaces are the same age.

The scarp profile P7 presented in Fig. 6 was obtained on surface s1, uplifted between 18 m and 19 m at this place. This profile was levelled in a portion of the scarp preserved from runoff

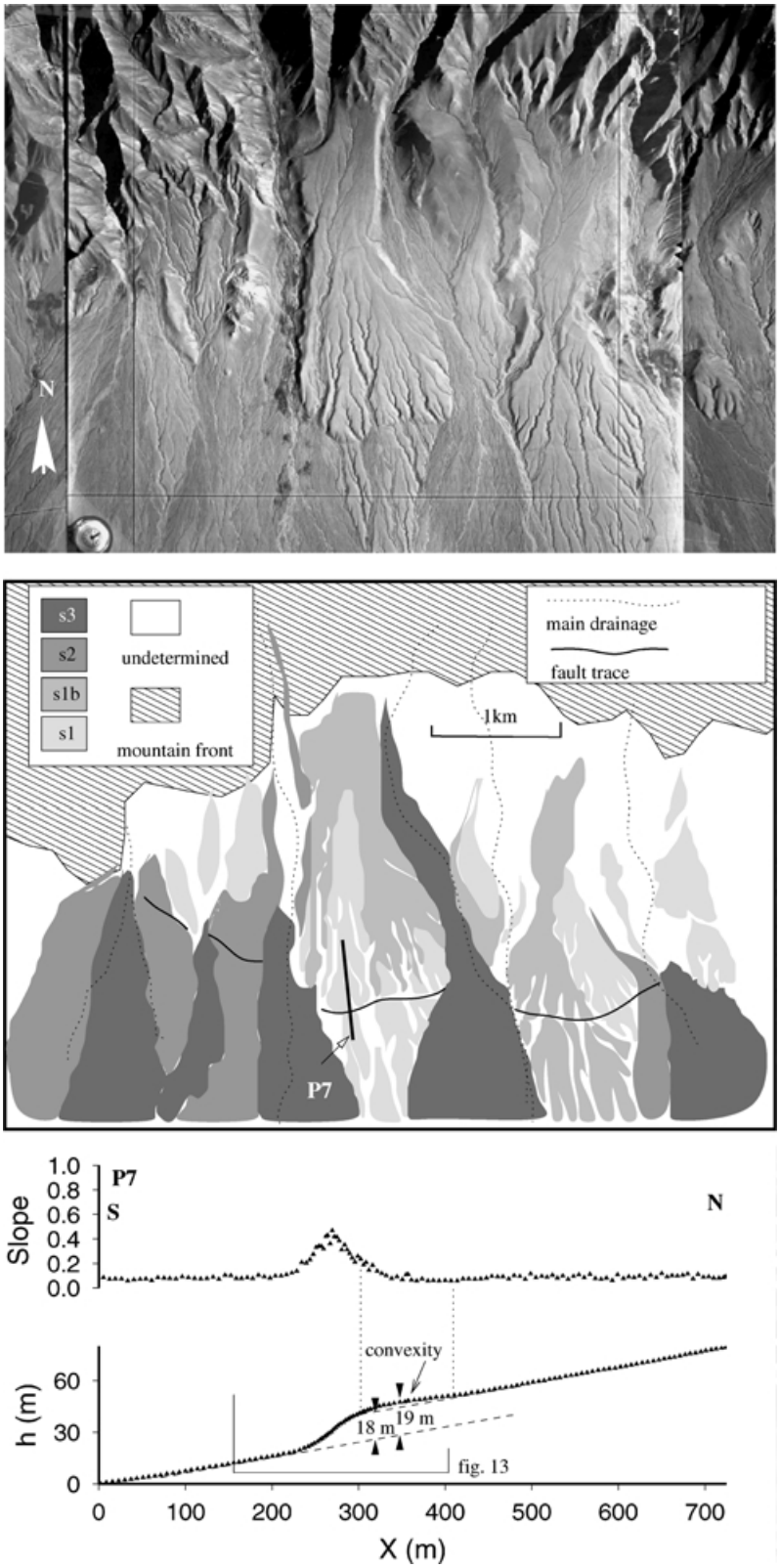

Figure 6. Geomorphic analysis of aerial photos along the thrust SE of Baga Bogd (see Fig. 1 for location). We identified 4 alluvial surfaces from their relative elevation and field observations. The oldest and more uplifted surface s1 corresponds to a debris flow surface. Surface s1b is embedded in s1 and we interpret is as a wash surface. Surface s2 correspond also to a debris flow surface embedded in s1 and s1b. Surface s3 corresponds to the youngest deposit and is unaffected by the thrust, showing that this fault has not broken the surface from the deposition of s3. The black line indicates the location of the scarp profile P7. This profile was levelled in a portion of scarp not altered by runoff driven processes. Elevation profile shows a convexity at the top of the scarp which is interpreted as morphological effect of folding. The maximum cumulative offset including the folding component is 19 m. The cumulative offset associated with faulting only is $\leq$18 m.

processes. Profile P7 has a roughly symmetric shape that we do not observe on profiles levelled along the Gurvan Bulag thrust scarp (see also the field photograph, Fig. 2e). This morphology can be explained by a fixed fault cutting the surface at the inflection point of the elevation profile. A convexity appears on the elevation profile between x ∼290 m and x ∼ 400 m (Fig. 6). This convexity is interpreted as a morphological consequence of folding. No obvious surficial trace of a backthrust can be observed in association with this convexity, but it may have disappeared by erosion from the cessation of the seismic activity. Because of the folding component of the offset, the slope profile shows two populations, separated at x ∼ 290 m (Fig. 6). Unlike our interpretation along the Gurvan Bulag fault scarp, these two populations do not correspond to variable locations of the fault responsible for the surface rupture. The maximum cumulative offset including the folding component of the uplift is estimated at 19 m (Fig. 6). The cumulative offset corresponding to the approximation of the hangingwall surface by a planar surface is 18 m (Fig. 6). This offset is an estimate of the uplift component due to faulting only.

2.3 General implications for the morphological evolution of forebergs

The observed variability of topographic expression associated with reverse faulting seems to be related to cessation of alluvial deposition and evolution of the fault system itself. The repetition of earthquakes increases the surface deformation, so that the thrust scarp eventually forms a topographic ridge, which can act as a barrier to sedimentation (Fig. 7a). However, for a scarp to achieve this morphology it must be located either far from outwash channels of major drainage basins, or to the side of them. When the thrust scarp is close to and in front of a major drainage basin outlet it is modified by processes including scarp abrasion and deposition, depending on the fluvial transport capacity and the sediment supply in the drainage basin (Carretier *et al.* 1998). These alluvial processes can cause destruction of the scarp or filling of the depression between the remnant scarp convexity and the range front (Fig. 7b), and may be influenced by climatic variations. The resulting uplifted alluvial surfaces can be flat (see profile P2, Fig. 5). Consequently, when the thrust scarp is far from main drainage basin, the wavelength of the deformation associated with thrusting is revealed by the distance between the scarp front and the toe of the alluvial deposits (Fig. 7a). However, when the scarp is in front of a main basin outlet, the distance between the thrust front and the alluvial deposits is controlled instead by successive erosion and deposition horizons (Fig. 7a). In principle, the wavelength over which incised channels and terraces form is also influenced by the down-dip fault length, as shown in numerical models of elastic displacement fields and diffusive geomorphic processes (Arrowsmith *et al.* 1996). In practice, the real wavelength of the deformation appears to be controlled by the location of backthrusts, which may correspond to a flattening of the thrust dip at depth (Fig. 7). The variation in apparent wavelength along the Gurvan Bulag foreberg ridge is more likely to be controlled by the scarp location relative to the main drainage basins than by lateral variations in fault dip. The scarp of Dalan Turuu, north of Ih Bogd, illustrates this conclusion (Figs 1 and 2b). This thrust scarp forms a topographic ridge 200–300 m high, with a constant width along the fault. No major drainage basin crosses the thrust.

In the second part of this study, we will model scarp profiles to estimate their morphological ages. These scarps are incised by locally-formed drainages and also thorough-going or antecedent drainages from the upstream fan sources. We will focus our study on portions located between incisions, where surfaces have been preserved from runoff processes by their offset. In these portions, the fault scarps are eroded only by slope processes which are the only processes taken into account in our modelling approach. We took profiles far enough from drainages to ensure that main gradient is oriented normal to the fault, so that 1-D modelling can adequately reproduce the main direction of sediment flux. We attempt to interpret the discrepancies between our model and the data according to the influence of other geomorphic processes that we can identify.

3 MODELLING APPROACH

Four approaches are possible to model the evolution of scarp morphology on active faults: 1) the scarp morphology is assumed to be controlled by elastic displacements of the surface related to dislocation at depth (e.g. King *et al.* 1988; Stein *et al.* 1988; Taboada *et al.* 1993); 2) the scarp is assumed to be controlled by surface rupture and slope erosion processes (e.g. Culling 1960; Nash 1981; Avouac 1993; Arrowsmith *et al.* 1998); 3) the scarp evolution is controlled by both effects 1 and 2 (e.g. Arrowsmith *et al.* 1996); 4) the scarp morphology is assumed to be controlled by slip between stratified deposits of different rheology (Nino *et al.* 1998). We chose the second approach which involves imposing the surface rupture and modelling the erosion of scarps using a linear diffusive analogue. We did this for several reasons: 1) our goal is to date scarps using the erosion of their morphology; 2) elastic dislocation models are very sensitive to the fault geometry and depth (King *et al.* 1988; Arrowsmith *et al.* 1996), which are not well constrained in our area. Therefore, the width of our topographic profiles is short (several 100 m) compared to the length of the faults (10–20 km), so the effect of the elastic dislocation modelling is diminished (Arrowsmith *et al.* 1996); 3) scarp morphology depends on interactions between successive alluvial deposits and the seismic cycle. In most of the cases we discuss, uplifted and preserved surfaces do not correspond to single surfaces that can be modelled by an elastic dislocation model.

Morphological dating is the process of comparing modelled and observed profiles to determine the age of the landform. We use a linear diffusion analogue to describe scarp erosion preserved from runoff processes (portions of fault scarps located between incisions). In this case, the transport law is that the local flux of sediments is proportional to the local topographic slope (Culling 1960). We assume that material of faulted alluvial fan has been always available for transport. This is consistent with non-cohesive alluvial sediments observed on the field. Thus, assumption of transport limited conditions and application of the continuity equation for sediment flux will result in a diffusion-like equation relating the local erosion rate and the local topographic curvature ($\frac{\partial h}{\partial t} = \kappa \frac{\partial^2 h}{\partial x^2}$, where h iselevation at point x, and t the time). The proportionality coefficient κ [in unit of $m^2\ ka^{-1}$] is called the diffusion coefficient. By fitting synthetic topographic profiles computed with these assumptions to observed scarp profiles we can estimate the product κt where t is the age of the scarp. We will call this product the "morphological age" of a scarp.

Dating scarps becomes more uncertain when repeated faulting is involved, as Avouac & Peltzer (1993) show for cumulative normal fault scarps. In this case the unknown parameters controlling erosion and tectonics are multiplied by the number of events. This is even more difficult in the case of cumulative reverse faults because of the variability of the surface faulting itself. Numerous descriptions of trenches across reverse active faults show that the position of the

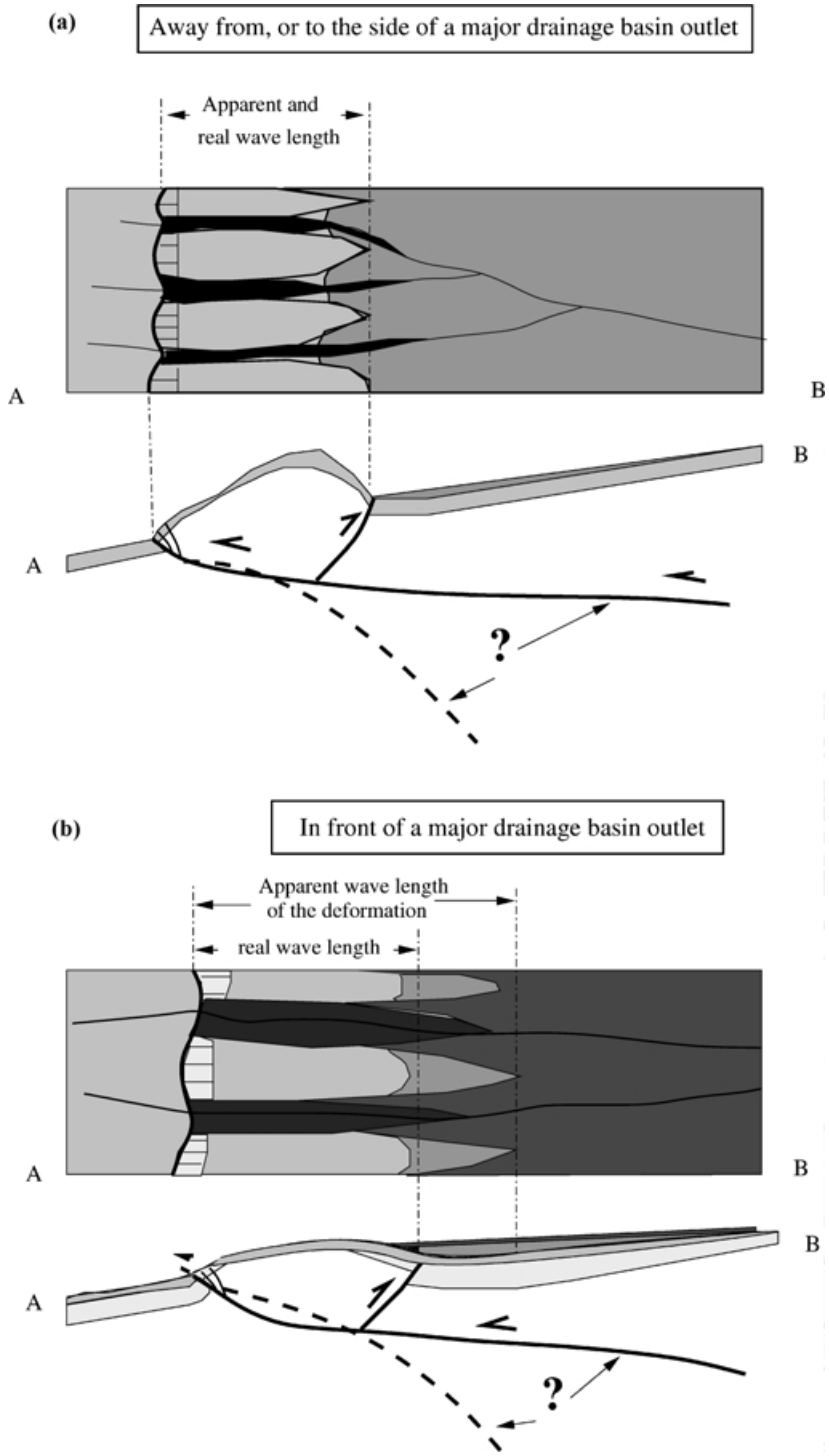

Figure 7. Conceptual sketches that illustrate alluvial sedimentation contexts and foreberg morphologies. (a) When the foreberg is away from a major drainage basin outlet, the geomorphic limit between alluvial surfaces is mainly controlled by the development of a folded and backthrust ridge that forms a barrier to sedimentation. In this last case, the distance between the fault trace and the lower limit of recent fans shows the true wavelength associated with the folding and backthrusting. (b) However, when the foreberg is located in front of a major drainage basin outlet, the fluvial transport (abrasion or sedimentation) tends to level the regional scarp slopes. Limits between alluvial geomorphic surfaces in map view are mainly due to the interplay between stream incision and the development of terraces rather than the surface displacement due to folding and backthrusting.

rupture at each event is usually variable, unlike most cases of normal faulting (see for example McCalpin, 1996, pp. 107–211; Meghraoui *et al.* 1988; Swan 1988; Philip *et al.* 1992; Yeats *et al.* 1997, p. 352). Along the Gurvan Bulag ranges, the position of the 1957 event trace at the base of cumulative scarps and trench observations suggest that the rupture steps forward in each event (Figs 2 and 5). Hanks *et al.* (1984) proposed a simple analytical model for dating cumulative scarps, involving diffusion of continuous uplift on a fixed and vertical fault. His model cannot be applicable in such cases.

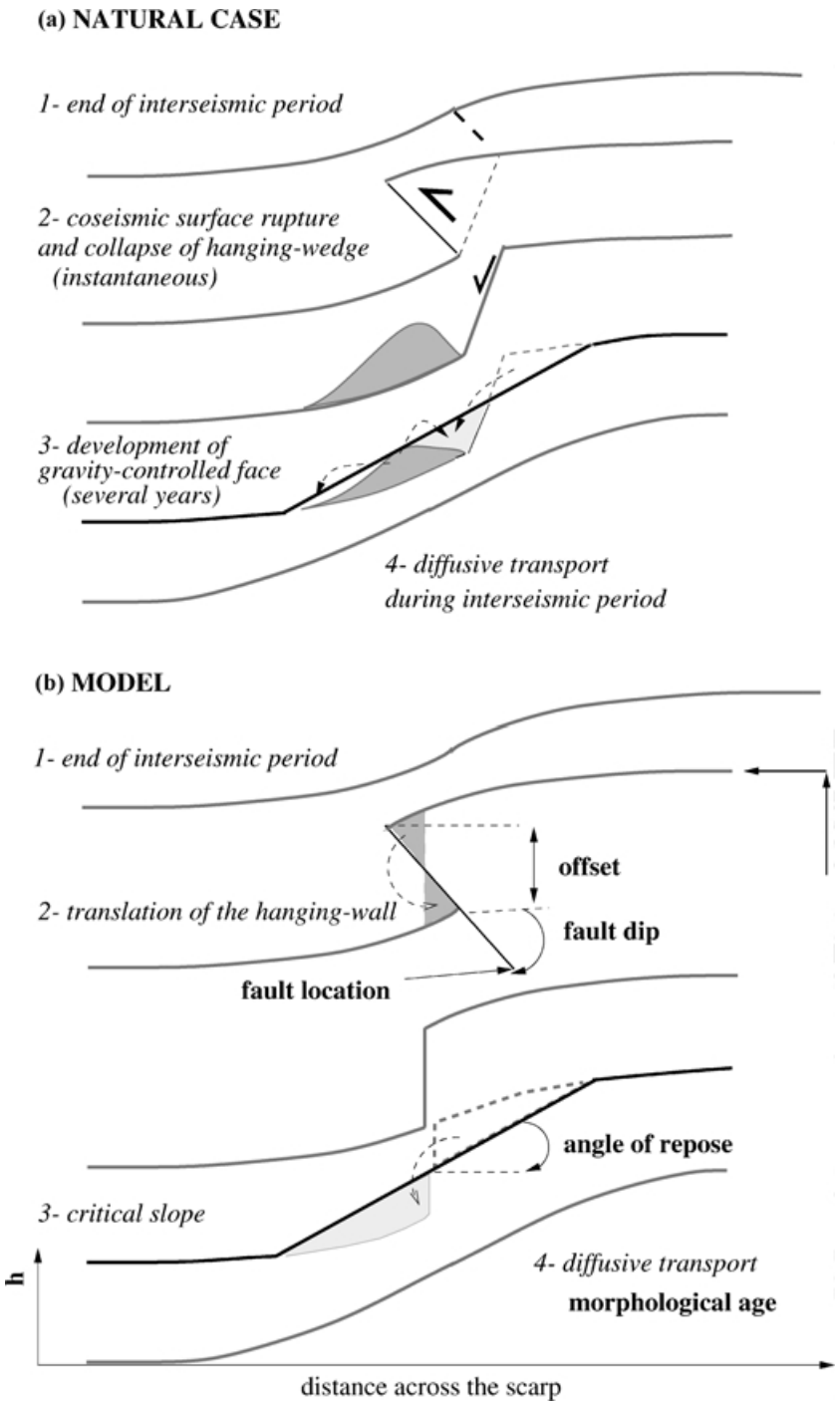

Figure 8. Modelling of reverse faulting and scarp erosion. (a) Natural case. Three stages can define the geomorphic evolution of a reverse fault scarp: (1) instantaneous collapse of the hanging wedge due to reverse movement, (2) development of a gravity-controlled face at the angle of repose of the material over several years. At the end of this stage, material is equally distributed between hangingwall and footwall. 3) Diffusive transport. (b) Model. The surface rupture is modelled by a translation of the profile in the hangingwall according to specified dip of fault and vertical offset and from the middle of the hanging-wedge. The gravitational collapse is modelled by reducing all slopes greater than the specified slope of repose. These two steps preserve the mass-balance between hangingwall and footwall. Linear diffusion is then applied during a specified morphologic duration ($K\Delta t$).

We thus introduced some extra complications in our model allowing the position of each rupture, which can be variable in each event, and the fault dip at the surface to be specified (Fig. 8). We also allow the surface slope to collapse after a surface rupture when the slope exceeds the slope angle of repose of the non-cohesive material. In that sense, our model is similar to the model used by Avouac & Peltzer (1993) for cumulative normal fault scarps. Gravity-controlled failure of scarps has been well described and is common when faulting occurs in non-cohesive material (Wallace 1977; Machette 1987) leading over several years to a gravity-controlled face that forms after the collapse of the hangingwall-wedge by a normal fault whose position can be

variable (McCalpin 1996, p. 200) (Fig. 8a). The gravitational collapse is not a diffusive process. It is driven by internal friction of unconsolidated material (Roering *et al.* 1999). Thus, when the scarp slope reaches a threshold slope (or "slope of repose"), it collapses quickly. We observed that this process is a strong controlling factor of scarp evolution. For example, Fig. 2A and profile P5 (Fig. 5) show a cumulative reverse fault scarp for which the frontal portion collapsed during the 1957 event. This process affected a large part of the scarp, which consequently lost its diffusive morphology. The resulting gravity-controlled face will then erode by diffusion until the next surface rupture. The future diffusive morphology will only provide information about the age of the 1957 event. Consequently, it is clear that this process is a strong limitation for dating of the initiation of uplift. Along the Gurvan Bulag range, the vertical height of the gravity-controlled face acquired several months after the 1957 dislocation is variable, even between places separated by only a few hundred of metres (compare for example profiles P5 and P2, Fig. 5). These observations show that slope collapse can refresh reverse fault scarp morphology to varying degrees, and consequently it must be taken into account in our morphologic dating model. Some authors used forward modelling in which gravitational collapse is computed at the same time as diffusion (e.g. Arrowsmith *et al.* 1998). This is very useful to estimate slip rates when processes are demonstratively continuous. In the case of repeated faulting with large offsets, the possible variation of the surface rupture location and the variable degree of frontal collapse impose to respect the succession of geomorphic processes.

In summary, we model topographic scarp profiles as follows (Fig. 8a):

(i) we chose the position of the surface rupture and of the dip of the fault;

(ii) we specify the offset on the fault;

(iii) we simulate the initial collapse of the hangingwall by forming a vertical step in the middle of the offset (Fig. 8b). This choice allows to preserve the mass-balance between eroded material from the hangingwall and the deposited sediment in the footwall at the end of the next modelling step, whatever the position of the normal fault is, until its dip is greater than the critical slope (Fig. 8b). This modelling preserves the shortening associated with the reverse component.

(iv) We allow the slope to collapse under gravity in order to bring the scarp slope to the angle of repose of the material ($\sim 30^\circ$). To achieve this we apply diffusion with very high diffusion coefficient to slopes exceeding the slope of repose (Andrews & Hanks 1985). Although gravitational collapse is not a diffusive process, this numerical method enables to respect mass balance of transport. It also enables us to reduce slope instantaneously by using a sufficiently high diffusion coefficient. The transport-limited condition implies that this process affects all slopes greater than the angle of repose, and thus that the free face formed just after the earthquake is very quickly degraded. This is consistent with our field observations.

(v) A linear diffusion equation is then solved by "forward time central space" finite difference method over the imposed duration of the interseismic period (Δt).

Synthetic cumulative scarps profiles are calculated by repeating these four stages. For each time period, defined by either tectonic displacement, gravitational collapse or diffusive erosion, we can impose the values of vertical offset, fault dip and position, slope angle of repose, diffusion coefficient and duration between events (both included in the term $\kappa \Delta t$).

4 THEORETICAL RESULTS

Fig. 9 illustrates schematically two extreme cases observed in our numerical experiments. They differ by the relative magnitude of parameters. The inherited diffusive scarp morphology may or may not be preserved when a new seismic event occurs. This depends on gravity-driven processes that tend to maintain scarp slopes at the angle of repose of detritic material, resetting the diffusive scarp morphology. In terms of morphological dating, such resetting is equivalent to resetting the clock. Indeed, large offsets and repeated surface rupture at the same place (Fig. 9, case A) enhance the development of a gravity-controlled face. In this case, the gravity-controlled height exceeds the true value of the vertical component associated with a single surface rupture. As mentioned previously, such behaviour has been observed along the Gurvan Bulag range (see Fig. 2a and profile P5 on Fig. 5). This effect can have important implications in palaeoseismology, as well as for scarp morphology and dating. When estimating the vertical component of a surface rupture from the total vertical height of the gravity-controlled face, this effect will lead to an overestimate of the last vertical offset. This suggests that 1957 offsets along the Gurvan Bulag range could have been overestimated by Kurushin *et al.* (1997) when using height of the gravity-controlled face (e.g. Kurushin *et al.* 1997 site 17, p. 99), and some cumulative scarps considered previously as one event scarp could be in fact two-events scarps (see for example profile P4 in Fig. 5). By contrast, distinct forward-stepping faults with small offsets preserve the diffusive scarp morphology (Fig. 9, case B). Between these two extremes cases, we obtained a lot of different morphologies which can not be summed up in a general graph. These morphologies differ by their relative record of past events. Thus, preservation of diffusive morphology depends on local factors which must be evaluated in the field and by modelling.

Consequently, it is clear that dating the beginning of the ramp formation is not always possible. In the worst cases, we can only date the penultimate event (in this case, the event before 1957). For example, our theoretical simulations of ruptures localized on a 45° dipping fault suggest that incremental offsets greater than 3 m will imply a total resetting of the diffusive scarp at each event, whatever values the other parameters have. This is in contrast to the case of repeated normal faulting. Although development of a gravity-controlled face can occur in both cases, in normal faulting the increase of the scarp length (distance between two symmetrical points in the hangingwall and in the footwall) preserves diffusive scarp morphology.

5 BEST fiTTING MORPHOLOGICAL AGE DETERMINATION

In order to determine the best fitting values of morphological age for the different processes, we performed a parameter search by forward modelling in which $\kappa \Delta t$ (product of diffusion coefficient and interseismic duration) is incremented, and for each value the root mean square of the misfit between observed and modelled elevation profiles is calculated (Avouac 1993; Arrowsmith *et al.* 1998):

$$\mathrm{RMS} = \sqrt{\frac{1}{n}\sum_{j=1}^{n}(h_{\mathrm{modelled}}(x_j) - h_{\mathrm{observed}}(x_j))^2} \qquad (1)$$

where n is the number of points x_j of the observed profile.

The RMS versus $\kappa \Delta t$ passes through a minimum $\mathrm{RMS}_{\mathrm{min}}$ which corresponds to the best fitting $\kappa \Delta t$. In order to estimate a confidence

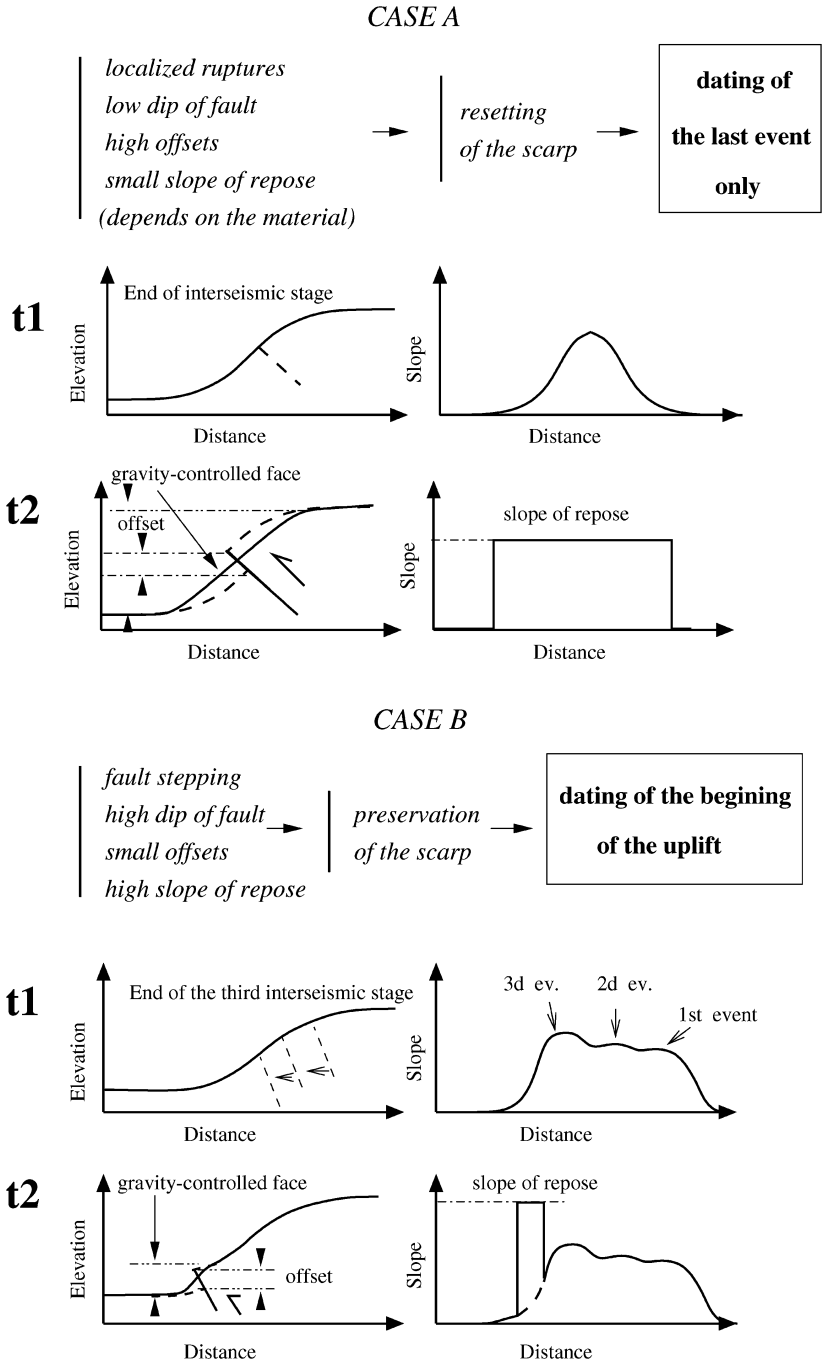

Figure 9. Schematic results of numerical modelling for two extreme cases. In case A the reverse component of faulting removes a part of inherited diffusive morphology at each event so that gravity-driven collapse of slope after each surface rupture resets the diffusive fault scarp morphology. Repeated localization of the rupture in the same place and high incremental offsets enhance this effect. Consequently, the vertical height of the gravity-controlled face exceeds the value of the incremental offset. In case B, forward stepping of successive dipping faults and low incremental offsets values preserve the diffusive scarp morphology.

interval of the inferred age, we related the range of acceptable fittings to the RMS values lower than $\mathrm{RMS}_{\min} + 5$ cm. By doing this, we retained the same criterion proposed by Avouac (1993) and used by other authors (e.g. Avouac & Peltzer 1993; Arrowsmith *et al.* 1998). This criterion has been used to determine an objective estimation of the precision with which morphological ages are estimated, taking into account topographic levelling with precision of about 5 cm. In that sense, if several models can match the same data with RMS lower than $\mathrm{RMS}_{\min} + 5$ cm, they will not be differentiated. The levelling of our profiles has been made by differential GPS method which is accurate to less that 5 cm. Consequently, this value is adapted to define confidence intervals of morphological ages estimated in this study. This criterion allows us to determine the values $\kappa\Delta t_{\min}$ and $\kappa\Delta t_{\max}$ corresponding to values of $\kappa\Delta t$ at the intersections between the RMS curve and the horizontal line defined by $\mathrm{RMS} = \mathrm{RMS}_{\min} + 5$ cm. We define the morphological age by $\frac{\kappa\Delta t_{\min} + \kappa\Delta t_{\max}}{2}$ and its uncertainty by $\kappa\Delta t_{\max}$ minus the morphological age. When converting morphological ages into diffusion coefficient, we propagate the uncertainty associated with each parameter as follows: considering that $\delta\kappa t$ and δt are the uncertainties associated

with values of κt and t respectively, then κ is given by $\frac{\kappa t}{t} \pm \delta\kappa$, where $\delta\kappa$ is $\sqrt{(\frac{\delta\kappa t}{\kappa t})^2 + (\frac{\delta t}{t})^2}$ (Bevington & Robinson 1992). We apply the same method to convert morphological ages into numerical ages or slip rates.

Morphological age is not the only parameter which controls the accuracy of fittings between observed and modelled profiles. The determination of the best fitting morphological age and uncertainty requires estimation of several parameters such as number of events, the incremental offsets, the dip of the faults, their location, the angle of repose of material, and the regional (initial) slope of the profile. Some of these parameters can be evaluated from field data, namely the regional slope corresponding to the portion of profile far from the scarp, and the angle of repose which is given by the portion of the scarp associated with the 1957 event. Other parameters are more difficult to determine. For example, the dip of the faults and their location remained uncertain in most of the cases. A trench across a fault scarp, which is necessary to determine the fault geometry, has not always been possible, especially when scarps are several metres high. Consequently, the solution given for each modelled profile should not be unique. Therefore, estimated morphological ages and their uncertainty should depend on the assumptions made about fault geometry, values of incremental offsets and number of events. Keeping this in mind, we fix these parameters using morphological arguments, and compare our results with previous estimations of slip rates and time recurrence intervals based on cosmogenic dating of uplifted surfaces in our study site (Ritz *et al.* 1999).

We assume that the interseismic duration Δt and the diffusion coefficient κ are constant, so that RMS is computed with constant $\kappa\Delta t$. As Arrowsmith *et al.* (1998) as well as others showed (e.g. Nivière & Marquis 2000), the uncertainty of morphological age increases with the age of the scarp. Consequently, the single value of $\kappa\Delta t$ relative to a past event can not be resolved with a good accuracy (see Appendix A, Fig. A1c). On the contrary, constant $\kappa\Delta t$ between events allows us to estimate a best fitting value with a good accuracy (see Appendix A, Fig. A1c). The best fitting value of $\kappa\Delta t$ that we compute has consequently the sense of a mean value, which gives mean dating and uplift rate.

We assume that the incremental offsets are equal to the local value associated with the 1957 event (Kurushin *et al.* 1997), and in this sense the successive events are "characteristic" as suggested by Ritz *et al.* (1999) and Kurushin *et al.* (1997). Consequently, to estimate the number of events, we divided the cumulative offset by this incremental offset.

We assume that the fault responsible for the surface ruptures steps forward at each event. We have no direct evidence of this behaviour for the studied profiles because it has been impossible to trench across scarps which can reach 20 m height. However, some other trenches across reverse fault scarps around the Gurvan Bogd range displayed such pattern, while some other showed unique faults or more complex geometry (Bayasgalan *et al.* 1997; Bayasgalan 1999). We argue for a forward stepping of the faults from the scarp morphology: first, the portion of the scarp associated with the more recent event (1957) is generally located at the front of scarps (Fig. 5); secondly, slope distribution across scarps is usually not symmetrical, and slope decreases upwards from the position of the last rupture (Fig. 5). This suggests that the upper part of scarps is more degraded and thus older than the lower one. Such morphology may also result from the ridding of the hangingwall over the land surface by the way of a flat fault, prolongating a shallow ramp fault geometry. In this case, the frontal part of the scarp would correspond to the propagating flat fault. Thus, the slope of the frontal scarp would be lower than the slope of repose of the material, especially in the case of one event scarps. Nevertheless, all our profiles display a slope at the front of the scarp ($\sim$0.7) which corresponds to classical values for slope of repose of detritical sediments (e.g. Wallace 1977; Machette 1987; Avouac & Peltzer 1993) (Fig. 5). Although this hypothesis can not be rejected by direct evidence, morphological arguments seem to favour the stepping of successive faults.

To determine the location of the successive faults responsible for the surface rupture requires one to look at slope profiles. A surface rupture associated with a seismic event causes an abrupt perturbation of the slope profile. When a surface rupture is followed by an interseismic period this perturbation acquires a "Gaussian" shape, that is predicted by a diffusion model (Fig. 9 case A, slope profile) (Avouac 1993; Nivière *et al.* 1998). Assuming that their formation is only related to surface rupture, the identification of these "Gaussians" or inflections of a slope profile depends on the distance between the successive surface ruptures (compare Fig. 9 case A and case B). Consequently, we can estimate the location of the successive faults from the slope profile independently of the morphological age, in such a way that the locations of observed and modelled slope inflections fit.

The dip of faults is one of the parameters controlling the gravitational collapse of the scarp, and thus the preservation of the diffusive scarp morphology (Fig. 9). This parameter cannot be evaluated in this study. However the estimation of the best fitting morphological age does not depend on this parameter when the morphology associated to past events is preserved (see Appendix A, Figs A1a,b).

The successive steps of our fitting method are the following:

(i) The incremental offset and the number of events are estimated from the elevation profile, and the slope of repose and the regional slope are estimated from the slope profile. The slope of repose is estimated from the mean slope of the gravity-controlled face rather than local maximum.

(ii) The successive fault locations are estimated from the slope profile. The fault dip is taken arbitrary lower than vertical (50°) to reduce the uncertainty of the best fitting morphological age (see Appendix A).

(iii) Forward modelling assuming non-vertical faults is carried out to evaluate if the scarp could have been reset during the uplift. This step aims at determining whether the initiation of the uplift or only the last events can be dated (see Fig. 9).

(iv) The RMS is calculated for different values of $\kappa\Delta t$ and the best fitting morphological age and its associated uncertainty is determined graphically.

We apply this methodology to the examples previously described. In each case, the RMS between observed and modelled profiles is computed only on the apparent diffusive portion of the scarp.

6 EXAMPLES

6.1 The Gurvan Bulag reverse fault (Figs 1, 3 and 4)

As mentioned earlier, cosmogenic dating of uplifted alluvial fans allowed Ritz *et al.* (1999) to propose that seismic activity resumed on this fault from at least the deposition of surface s3 dated at 12.7 ± 1.95 ka. By the morphological dating of cumulative reverse fault scarps, we want to date the beginning of the uplift of the older surface s2 (deposition at 118.6 ± 17.8 ka, Ritz *et al.* 1999).

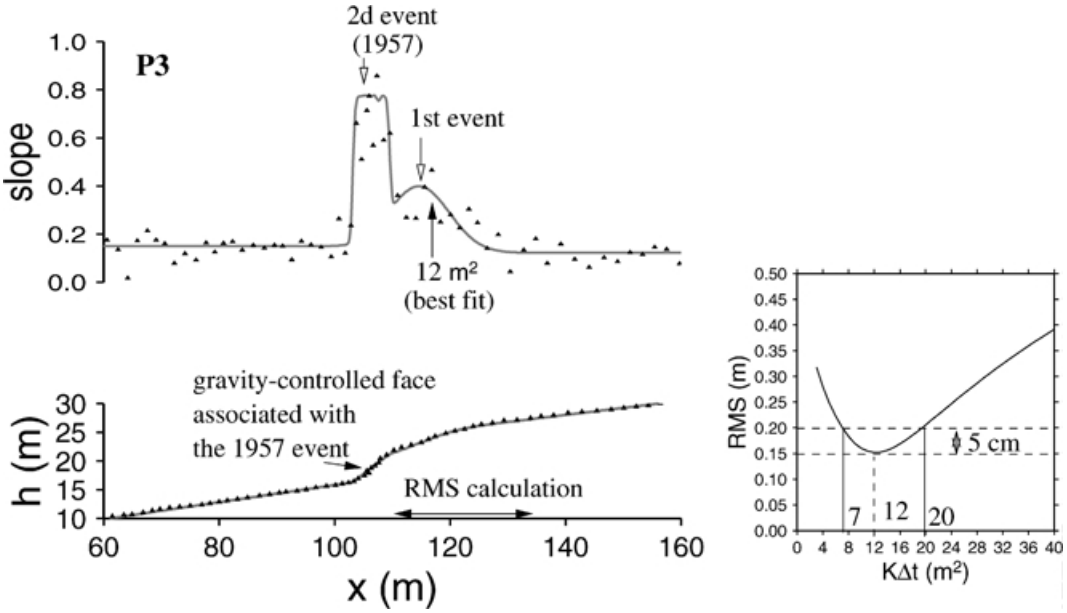

Figure 10. Morphological dating from Profile P3 (see Fig. 4 for location). Triangles are data and solid lines are models for the best fitting morphological age, using two events of 3.2 m offset on faults dipping 50° with 10 m distance between the two slip surfaces. The best fitting morphological age and associated uncertainty is determined graphically from the RMS versus constant $\kappa\Delta t$. The RMS is calculated from the elevation data, over the length corresponding to the diffusive morphology (horizontal arrow on the elevation profile). To define the range of acceptable values of $\kappa\Delta t$, we retain all models for which the RMS lies between RMSmax and RMSmin +5 cm (see text for details).

6.1.1 Profile P3 (Figs 4 and 10)

This profile is levelled across surface s4, uplifted 6.5 m (Fig. 10). This cumulative offset is twice the vertical offset of the 1957 event (3.25 m). The gravity-controlled face associated with the 1957 event is located at the front of the scarp, allowing to preserve the diffusive morphology associated with the last interseismic period. Using two events (including the 1957 event), with faults dipping 50° and 10 m apart, morphological ages determined from the RMS range from $\kappa\Delta t = 7$ to 20 m^2 (Fig. 10). The mean morphological age of the penultimate event is thus 13.5 ± 6.5 m^2. Ritz *et al.* (1999) estimated the age of the uplifted surface s4 at this place to be 4.1 ± 0.7 ka, based on cosmogenic measurements. It allows us to calibrate the coefficient of diffusion κ in our model at $\kappa = 3.3 \pm 1.7$ m^2 ka^{-1}, close to other estimates in the same climatic conditions (for example in the Dsungar desert located in Central Asia; Avouac & Peltzer 1993; Hanks 1999).

6.1.2 Profile P1 (Figs 4 and 11)

This profile is levelled across surface s2, uplifted between 14 m and 18 m (Figs 4 and 5). The gravity-controlled face is localized at the base of the scarp and most of the inherited diffusive morphology is preserved, allowing us to estimate the morphological age of the cumulative uplift (Fig. 9, case B). We identified on profile P1 the folding component of the uplift, which seems to not affect the slopes near the fault scarp (Fig. 5). Thus, we will estimate the morphological age of the scarp from the data located in the region presumably undeformed by folding ($x < 520$ m, Figs 5 and 11). The corresponding cumulative offset (14 m) is four times the local vertical offset associated with the 1957 event (∼3.5 m) (Fig. 11). The decreasing slope from the bottom to the top of the scarp and the frontal location of the gravity-controlled face suggest that the rupture stepped forward (Fig. 11). Using 4 events with 3.5 m offsets, and 15 m, 15 m and 12 m stepping of the successive faults (dipping at 50°) responsible for the surface ruptures, we estimate a mean $\kappa\Delta t$ ranging from 6.5 m^2 to 19 m^2 from the RMS curve ($\kappa\Delta t = 12.75 \pm 6.2$ m^2) (Fig. 11). This result is fairly consistent with the last morphological interseismic duration $\kappa\Delta t$ calculated from profile P3 (Fig. 10). The mean value of the morphological age at the profile P1 location (three interseismic periods) is 38.25 ± 18.6 m^2. If we use the coefficient of diffusion calibrated from the profile P3, we date the initiation of the uplift responsible of the cumulative offset of surface s2 at 11.7 ± 8.1 ka, and the penultimate event at 3.9 ± 2.7 ka. These estimates are consistent with 10Be dates (Ritz *et al.* 1999) as well as with preliminary results from palaeoseismological investigations giving the penultimate event at ∼4 ka (Schwartz *et al.* 1996; Bayasgalan *et al.* 1997). The uplifted surface s2 being dated at 118.6 ± 17.8 ka (Ritz *et al.* 1999), these results confirm that the seismic activity on the Gurvan Bulag fault resumed at ∼12 ka, and consequently, that this fault was almost quiescent between ∼118 ka and ∼12 ka. Over the last 11.7 ± 8.1 ka, we estimate from the 14 m cumulative offset of s2 an uplift rate on the Gurvan Bulag fault at 1.2 ± 0.8 mm yr^{-1}. This value is consistent with the previous estimate at 1.37 ± 0.25 mm yr^{-1} given by Ritz *et al.* (1999) for the same duration.

6.1.3 Profile P6 (Figs 4 and 12)

This profile is levelled across surface s2, uplifted 17 m, in front of a major drainage basin (Figs 4 and 12). Just as we detected 4 events on profile P1 responsible for the uplift the surface s2, we modelled the cumulative offset on profile P6 also using 4 events, with vertical incremental offsets of 4.25 m. The 1957 gravity-controlled face is located at the base of the scarp, suggesting a forward stepping of the fault. The slope profile shows a peak corresponding to the gravity-controlled face, followed by a roughly gaussian shape. Our numerical experiments suggest that the fault scarp collapsed

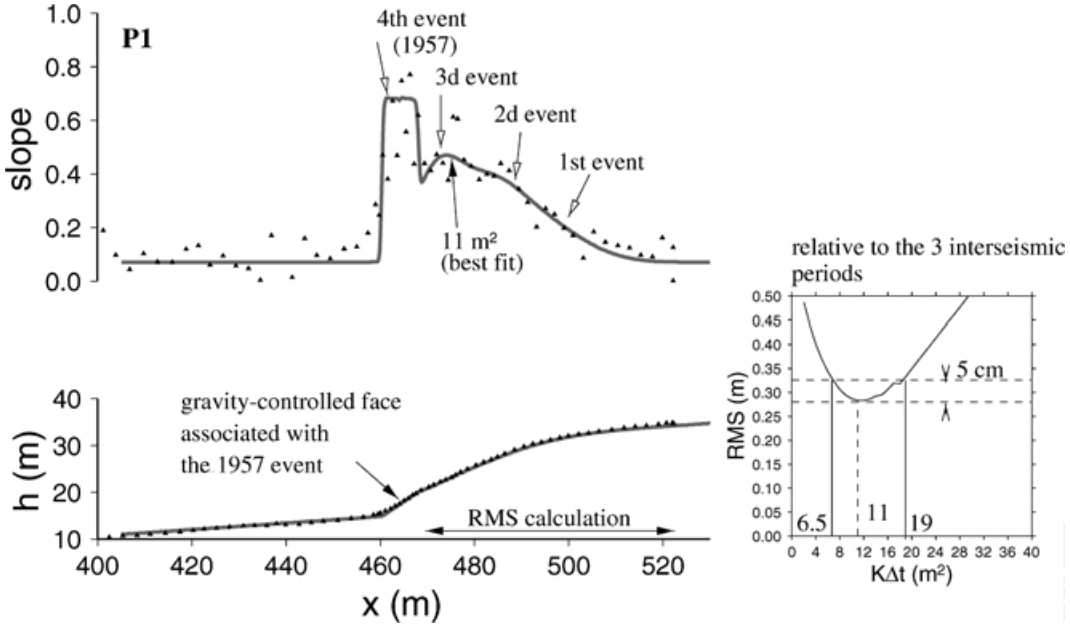

Figure 11. Morphological dating from profile P1 (see Fig. 4 for location). Triangles are data and solid lines are models for the best fitting morphological age, using four events of 3.5 m offsets on faults dipping at 50°, with 15 m, 15 m and 12 m distance between successive slip surfaces. The best fitting morphological age and associated uncertainty is determined graphically from the RMS versus constant $\kappa\Delta t$. The RMS is calculated from the elevation data, over the length corresponding to the diffusive morphology (horizontal arrow on the elevation profile). To define the range of acceptable values of $\kappa\Delta t$, we retain all models for which the RMS lies between RMSmin and RMSmin +5 cm (see text for details).

between each event prior to 1957. Coseismic scarp resetting occurs at each event because of the high offsets and because the fault steps at this locality (adjusted to fit the locations of inflexions on the slope profile) is smaller than at the location of profile P1 (Fig. 11). This occurs if we consider either faults dipping at 50° or vertical faults. Only the 1957 event allowed to preserve remaining diffusive morphology because it is located far from the penultimate rupture. This suggests that the remaining diffusive morphology has developed from the penultimate event, from a stage where the scarp was dominated by the stable gravity-controlled slope. Consequently, from the profile P6 we can estimate only the value of $\kappa\Delta t$ corresponding to the duration between the penultimate event and the 1957 event. This value is determined from the RMS curve at 21.5 ± 5.5 m^2 (Fig. 12). We tried to explain the slopes between x ~ 200 m and x ~ 240 m by a large stepping of the fault between the two first events. The fit of our synthetic slope to profile P6 requires a $\kappa\Delta t$ between the two first events greater than 150 m^2. This is inconsistent with $\kappa\Delta t$ calculated from profiles P3 and P1 ([6.5–20] m^2). Alternatively, we could interpret the slope profile between x ~ 200 m and x ~ 240 m as the folding component of scarp morphology that has no meaning in terms of morphological dating. Although the elevation profile P6 looks roughly linear after x ~ 250 m, folding seems to appear here, although we have no direct evidence.

Moreover, the morphological age of the penultimate event on profile P6 is much greater (21.5 ± 5.5 m^2) than in the previous estimates with profiles P3 (13.5 ± 6.5 m^2) and P1 (12.75 ± 6.2 m^2). In order to explain this, we suggest two possibilities: 1) the morphologic age calculated from profiles P1 and P3 could be underestimated. Folding tends to increase the scarp slopes and thus decrease the morphological age. 2) The estimate from profile P6 could be overestimated. While the folding can increase the scarp slopes, it can broaden the part of scarp profile apparently eroded, making it older morphologically. Therefore, offsets that we use to model the cumulative offset of P6 may also be too high (4.25 m for P6, compared with 3.5 m for P3). It is difficult to evaluate the contribution of folding to the cumulative offset on P6, because this folding is masked by alluvial sedimentation, that leads to a constant slope in the hangingwall. However, the cumulative offset estimated from profile P6 is similar to the maximum cumulative offset given by profile P1 (18 m). The maximum offset on P1 includes the folding component of the uplift, which appears more clearly than for profile P6. If our estimates of offsets are higher than the real ones, we will overestimate the morphological age (for two scarps with different offsets but with identical degradation states, the diffusion model will predict higher $\kappa\Delta t$ for the greater offset).

The overestimate due to folding and offset values is likely to be predominant here. We base this choice on the consistency between calculations in the two first profiles (P3 and P1), and because we know from numerical experiments that offset values have a strong influence on age estimates (Avouac 1993).

6.2 E-W thrust scarp to the south of Baga Bogd (Figs 1 and 6)

We stated from the previous geomorphic analysis of uplifted alluvial fans, that this fault has not broken the surface from the deposition of the more recent surface s3 (Fig. 6). A far as we do not have numerical dating of the uplifted surfaces, can we bound the age of the last event by morphological methods?

6.2.1 Profile P7 (Figs 6 and 13)

The symmetric shape suggests that rupture has remained localized near the inflection point of the scarp profile. The curved trace of the fault in plan view suggests that the fault has a relatively low dip (Fig. 6). We also have no clear indication of local incremental offset values, this scarp being unaffected by the 1957 earthquake.

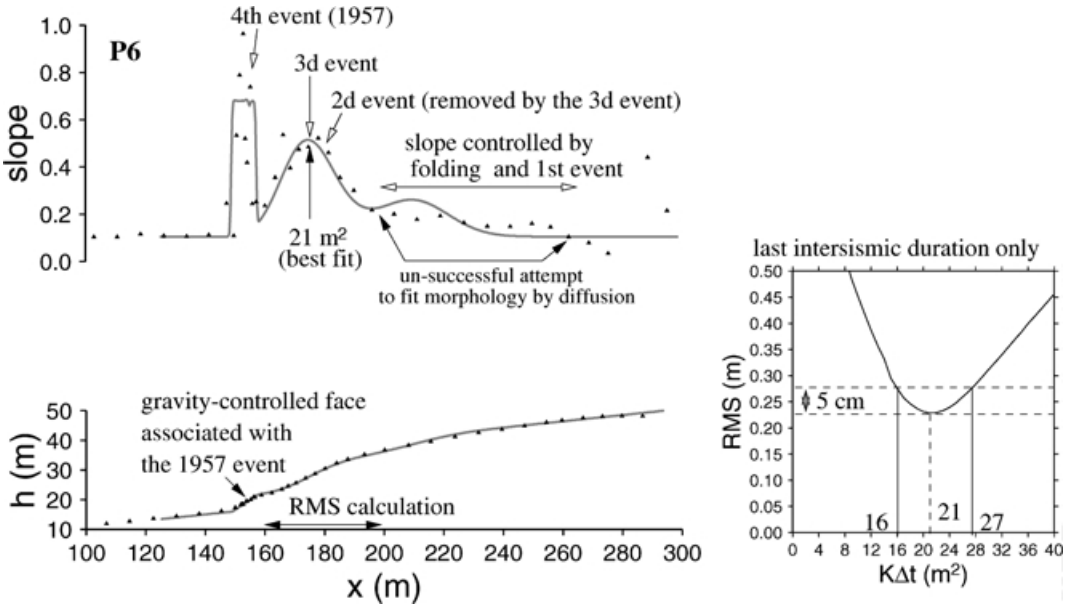

Figure 12. Morphological dating from profile P6 (see Fig. 4 for localization). Triangles are data and solid lines are models for elevation and slope profiles. The models correspond to four events of 4.25 m offset on faults dipping at 50° (see text), and successive interseismic durations of $\kappa\Delta t = 100$, 21 and 21 m^2. Using faults 40 m, 10 m and 27 m apart to respect the location of inflections of the slope profile, the modelling suggests that the fault scarp collapsed at the time of the third event. Consequently, we can only estimate $\kappa\Delta t$ corresponding to the last interseismic duration. Modelling suggests that it corresponds to the Gaussian shape of the slope gradient profile. The RMS between observed (elevation) and modelled profiles is thus calculated only for this part of the elevation profile (horizontal arrow on the elevation profile). To define the range of acceptable values of $\kappa\Delta t$, we retain all models for which the RMS lies between RMSmin and RMSmin +5 cm (see text for details). The first step of 40 m is a un-successful attempt to explain the slopes between 200 m and 240 m. In fact we interpret this part of the profile to be caused by the folding component of the scarp morphology.

The morphology between x ∼ 300 m and x ∼ 400 m is controlled by folding (Fig. 6). The cumulative offset associated with faulting is estimated at 18 m (Fig. 6).

We postulate that incremental offsets are similar in size to those at Gurvan Bulag with a maximum at ∼5 m. We carried out experiments varying the incremental offset between 3 and 5 m (corresponding to 6 and 4 events responsible for the cumulative offset of 18 m), the dip of the fixed fault between 45° and 90°. We fixed the value of the slope of repose at 0.7, which corresponds to the slope of the gravity-controlled face commonly observed for similar sediments along the Gurvan Bulag scarp. Such range of parameters implies the total removal of the synthetic scarp after two or three events, because of gravitational collapse associated with the reverse component and the large offsets (Case A of Fig. 9). Consequently, we can only date the last event from this scarp. To explain the observed smooth morphology, this scenario requires a long period of quiescence during which the fault is inactive. We date the last event at 235 ± 39 m^2 (Fig. 13). This morphological age is determined from the RMS versus $\kappa\Delta t$ computed over the portion of the scarp profile presumably unaffected by folding (x $\leq$ 290 m, Figs 6 and 13). This tends to reduce the possible overestimate of the morphological age due to folding, which is expressed morphologically at the upper part of the scarp. If we use the diffusion coefficient calibrated on the Gurvan Bulag Fault (which has the same orientation and same materials), we date the last event occurring on the Southern Baga thrust at 71 ± 38 ka. The uncertainty is large, but this age may correspond to the pause in surface rupture activity observed in Gurvan Bulag between approximately 118 ka and 12 ka. The resumption of surface faulting observed along the Gurvan Bulag scarp in the last 12 ka seems to have not occurred SE of Baga Bogd.

7 DISCUSSION AND CONCLUSIONS

The examples that we described illustrate a variability that depends on the balance between four processes (Bayasgalan *et al.* 1999a): 1) surface dislocation on faults, 2) folding associated with thrusting and backthrusting, 3) alluvial erosion and sedimentation, and 4) slope erosion. These factors have general implications for the morphological dating of any transport-limited reverse fault scarps.

7.1 Alluvial environment

Our examples suggest that cumulative reverse fault scarps can be dated when they are in front of drainage basins. In this case, climatically-controlled abrasion or deposition isolates surfaces that have been uplifted by different numbers of earthquakes. This alluvial environment controls the vertical growth of forebergs whose morphology is dominated by slope erosion.

7.2 Folding

Folding may decrease the apparent morphological age by increasing the scarp slope. It is difficult to quantify this effect. On the other hand, if folding is masked by sedimentation, producing flat topography (e.g. profile P2, Fig. 5), we may overestimate the fault offsets and therefore the morphological age of the scarp. A second effect which can lead to an overestimate of the morphological age is the surface bending associated with folding, which may be mistaken with diffusive-controlled morphology (e.g. Fig. 2f). The last two statements appear to be predominant. It is thus necessary to be very cautious about what controls the cumulative offset at each place. Sometimes analysis of natural cross-sections and of the scarp

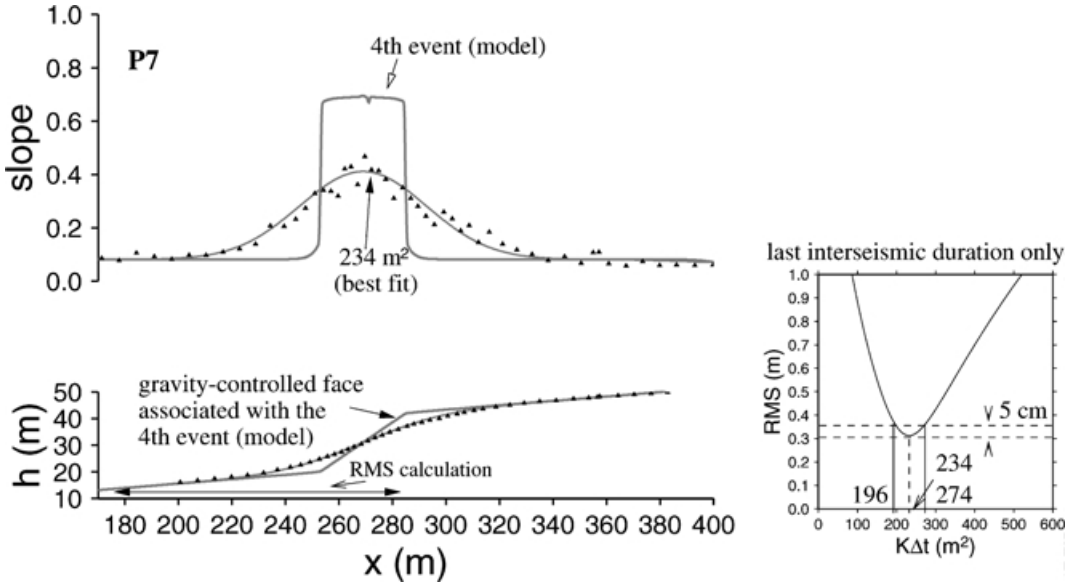

Figure 13. Morphological dating from the profile P7 (see Fig. 6 for localization). The symmetric shape of the elevation profile suggests that faulting has remained located at the inflection point of the scarp. Assuming a fault dipping at 45°, and 4.25 m offsets, the modelling suggests that the scarp collapsed at each event. Consequently, only the last event can be dated. The best fitting morphological age and associated uncertainty is determined graphically from the RMS versus constant $\kappa \Delta t$. The RMS is calculated from the elevation data, over the length corresponding to the diffusive morphology (horizontal arrow on the elevation profile). The right part of the profile (from x $\sim$ 300 m) is interpreted as folding. The RMS curve refers to the last interseismic duration only. To define the range of acceptable values of $\kappa \Delta t$, we retain all models for which the RMS lies between RMSmin and RMSmin +5 cm (see text for details).

gradient variation helps identify folding, even if it does not appear obviously on the scarp profile itself (profile P6, Fig. 12). Folding associated with reverse faulting could be present in all our studied profiles, leading in overestimated values of morphological ages. If so, our estimated morphological ages for large cumulative offsets (for which folding can affect significantly the dating) are maximum values. These values allow to bound the age of the initiation of the uplift, which is the aim of our study on the Gurvan Bulag fault. Moreover, the consistency of our results and previous estimations of uplift rates and resumption of the seismic activity on the Gurvan Bulag fault is encouraging (Ritz *et al.* 1999). Our study attempted also to test the application of morphological dating method to cumulative reverse faults scarps. We use a simple model to discuss the rule of several processes. To improve further works on such scarps, it will be necessary to add the folding in models for a more general parametrical analysis.

7.3 Distributed secondary faults

Trenches excavated in cumulative fault scarps can exhibit a main thrust with associated secondary fractures and colluvial wedges (e.g. Meghraoui *et al.* 1988; Philip *et al.* 1992). Other examples show a single fault cutting through alluvial deposits at each event (Figs 2d,f). Distributed faults within a scarp can cause several inflections of the scarp morphology at each seismic event. At the same time, folding may develop with variable amplitude (e.g. Philip & Megrhaoui 1993). When a cumulative fault scarp develops with large incremental offsets (>1 m), the resetting effect of gravitational collapse smooths surface irregularities and folding is only expressed in the morphology in the upper part of the scarp. In this case, the geomorphic evolution of a cumulative scarp is mainly controlled by the successive gravitational collapse after each event and diffusive slope erosion during interseismic periods. The morphology of scarps formed by small offsets is more sensitive to bending and distributed fractures because gravitational collapse is less efficient at removing variations at the surface in this case (Fig. 2f).

7.4 Reverse component, variable position of the main thrust, fault offsets and gravity-driven collapse

The morphology of cumulative reverse fault scarps is strongly controlled by gravitational collapse if faulting remains localized and if incremental vertical offsets are large (>1 m). Gravitational collapse and scarp shortening caused by the reverse component act to reset the diffusive shape. If a large part of the scarp is affected this reduces the number of unknowns by giving a new initial state of degradation at each event and by smoothing irregularities. On the other hand, such resetting removes information about the older events.

It is difficult to justify the use of analytical models that do not take this reverse component and its consequent gravity-driven collapse into account, unless this is demonstrably unimportant in that particular case. We prefer to used a forward model which, although simplistic, allows us to assess the importance of slope collapse by varying local parameters such as the slope angle of repose, the distance between successive faults and incremental rupture offset values. Our approach helps evaluate whether a whole scarp or only the penultimate event can be dated. Our model is, however, limited by the value of the cumulative offset. Beyond a certain offset, the morphology of scarp is only controlled by folding and incision.

A recent study pointed out that calibrated diffusivity on the shoreline of Lake Bonneville that non-linear diffusion matches the data better than linear diffusion (Mattson & Bruhn 1999). At the scale of hillslopes, Roering *et al.* (1999) showed also that erosion is better described by non-linear erosion. Non-linear erosion effects usually imply that the morphological ages estimated by linear diffusion will be overestimated. We expect that these non-linear effects

remain within the uncertainties relative to erosion parameters that we estimated.

7.5 Implications for the seismic behaviour of the Gurvan Bogd fault system

The complexity of the interactions between structure and erosion leads only to rough morphologic ages. However, this dating method allows us to bound the ages of scarps, and thus to improve the climatic and thrusting histories when it is associated with other dating methods such as cosmogenic isotope and thermoluminescence dating. On the Gurvan Bogd Range, we propose the following scenario:

(i) deposition of surface s1 at Pleistocene times south of Ih Bogd (synchronous with s1 of south Baga Bogd?);

(ii) thrusting of s1 and development of foreberg ridges $\sim$100 m high;

(iii) some time before 118 ± 7.8 ka the surficial tectonic activity stops on the Gurvan Bulag thrust;

(iv) fluvial transport with high capacity leads to the erosion of the scarp in front of the major drainage basin;

(v) deposition of surface s2 at 118 ± 17.8 ka south of Ih Bogd (Ritz *et al.* 1999);

(vi) at about 20 ka permafrost develops and then disappears at about 14 ka (Owen *et al.* 1998);

(vii) deposition of surface s3 at 12.7 ± 1.95 ka, south of Ih Bogd (Ritz *et al.* 1999);

(viii) around 12 ka, surficial tectonic activity resumes on the Gurvan Bulag thrust scarp, with four seismic events between then and the present day. The cosmogenic dating of the uplifted alluvial surface s3 allowed Ritz *et al.* (1999) to propose the resumption of the seismic activity after the deposition of this surface. Our study confirms that the Gurvan Bulag fault has been quiescent from $\sim$118 ka to 11.7 ± 8.1 ka. This is also consistent with the date propose by Owen *et al.* (1999) for the uplift of alluvial fans (10–13 ka);

(ix) earthquake of magnitude 8.3 in 1957.

The apparent seismic gap observed on the Gurvan Bulag thrust between $\sim$118 ka and $\sim$12 ka may correspond to the end of seismic activity that we interpret from dating the E–W thrust scarp SE of Baga Bogd (dated at 71 ± 38 ka). We thus confirm that tectonic activity on the thrusts of the Gurvan Bogd Range is not continuous but episodic (Ritz *et al.* 1999). Moreover, seismic activity on the different thrusts of the Gurvan Bogd range is not synchronous. Seismic activity resumes on the Gurvan Bulag thrust fault from the early Holocene, while it stopped before on the thrust located south east of Baga Bogd. This raises the general problem of how distributed faults move in a regional compressive strain field, and how seismicity is temporally distributed on major faults (see for example Wesnousky 1994; Stirling *et al.* 1996). In the Gurvan Bogd fault system, we observe a variation in fault behaviour with time that is seen in some palaeoseismicity studies and numerical models (Leonard *et al.* 1998; Huc *et al.* 1998; Ben-Zion *et al.* 1999).

ACKNOWLEDGMENTS

We are very grateful to R. Arrowsmith and G. Marquis for their careful reviews which improved this manuscript. We thank F. Lucazeau and H. Philip for reviews and discussions. We thank also J. Verdun and T. Hanks for discussions. A grant from the laboratoire de Géophysique, Tectonique and Sédimentologie (UMR5573) and from the Royal Society helped with fieldwork.

REFERENCES

Andrews, D.J. & Hanks, T.C., 1985. Scarp degraded by linear diffusion: Inverse solution for age, *J. geophys. Res.,* **90,** 10 193–10 208.

Armijo, R., Tapponnier, P. & Tong-Lin, H., 1989. Late Cenozoic right strike-slip faulting in southern Tibet, *J. geophys. Res.,* **94,** 2787–2838.

Arrowsmith, J.R., Pollard, D.D. & Rhodes, D.D., 1996. Hillslope development in areas of active tectonics, *J. geophys. Res.,* **101,** 6255–6275.

Arrowsmith, J.R., Rhodes, D.D. & Pollard, D.D., 1998. Morphologic dating of scarps formed by repeated slip events along the San Andreas Fault, Carrizo Plain, California, *J. geophys. Res.,* **103,** 10 141–10 160.

Avouac, J-P, 1993. Analysis of scarp profiles: evaluation of errors in morphologic dating, *J. geophys. Res.,* **98,** 6745–6754.

Avouac, J-P. & Peltzer, G., 1993. Active Tectonics in Southern Xinjian, China: Analysis of Terrace Riser and Normal Fault Scarp Degradation Along the Hotan-Qira Fault system, *J. geophys. Res.,* **98,** 21 773–21 807.

Avouac, J-P, Tapponnier, P., Bai, M., You, H. & Wang, G., 1993. Active thrusting and folding along the Northern Tien Shan and late Cenozoic rotation of the Tarim relative to Dzungaria and Kazakhstan, *J. geophys. Res.,* **98,** 6755–6804.

Baljinnyam, I. *et al.*, 1993. *Ruptures of Major Earthquakes and Active Deformation in Mongolia and its Surroundings*. Geol. Soc. Am., Memoir 181.

Bayarsayhan, C., Bayasgalan, A., Enhtuvshin, B., Hudnut, K.W., Kurushin, R.A., Molnar, P. &Olziybat, M., 1996. 1957 Gobi Altay Mongolia earthquake as a prototype for southern California's most devastating earthquake, *Geology*, **24,** 579–582.

Bayasgalan, A., 1999. *Active teconics of Mongolia. PhD thesis,* Cambridge University, Cambridge.

Bayasgalan, A., Berryman, K., Kendrick, K., Prentice, C. & Ritz, J-F, 1997. Palaeoseismological investigations along the 1957 Gobi-Altay, Mongolia, Earthquake Rupture: Preliminary results from Excavations along the Gurvan Bulag Thrust, *EOS Trans. Am. geophys. Un.,* **78,** 440.

Bayasgalan, A., Jackson, J., Ritz, J-F & Carretier, S., 1999a. Forebergs, flower structures, and the development of large intra-continental strike-slip faults: The Gurvan Bogd fault system in Mongolia, *J. Struct. Geol.,* **21,** 1285–1302.

Bayasgalan, A., Jackson, J., Ritz, J-F & Carretier, S., 1999b. Field examples of strike-slip fault terminations in Mongolia, and their tectonic significance, *Tectonics,* **18,** 394–411.

Ben-Zion, Y., Dahmen, K., Lyakhovsky, V., Ertas, D. & Agnon, A., 1999. Self-driven mode switching of earthquake activity on a fault system, *Earth planet. Sci. Lett.,* **172,** 11–12.

Bevington, P.R. & Robinson, D.K., 1992. *Data reduction and error analysis for the physical sciences*, 2nd ed., McGraw-hill, New-York.

Bierman, P.R., Gillespie, A.R. & Caffee, M.W., 1995. Cosmogenic ages for earthquake recurrence intervals and debris flow fan deposition, Owens Valley, California, *Science,* **270,** 447–450.

Bourlès, D.L., 1992. Beryllium isotopes in the Earth's environment, *Encyclopedia of Earth System Science,* **1,** 337–352.

Brown, E.T., Edmond, J.M., Raisbeck, G.M., Yiou, F., Kurz, M.D. & Brook, E.J., 1991. Examination of surface exposure ages of Antarctic moraines using *in situ* produced ^{10}Be an ^{26}Al, *Geochim. et Cosmochim. Acta*, **55,** 2699–2703.

Bucknam, R.C. & Anderson, R.E., 1978. Estimation of fault-scarp ages from a scarp-height-slope-angle relationship, *Geology,* **7,** 11–14.

Bull, W.B. & Pearthree, P.A., 1988. Frequency and size of quartenary surface ruptures of the Pitayacachi fault, northeastern Sonora, Mexico, *Bull. seism. Soc. Am.,* **78,** 946–978.

Carretier, S., Lucazeau, F. & Ritz, J-F, 1998. Approche numérique des interactions entre climat, tectonique et erosion. Exemple de la faille de Bogd, Mongolie, *Comptes Rendus de l'Académie des Sciences,* **326,** 1–7.

Culling, W.E.H., 1960. Analytical theory of erosion, *J. Geology,* **68,** 336–344.

Enzel, Y., Amit, R., Porat, N., Zilberman, E. & Harrison, B.J., 1996. Estimating the ages of fault scarps in the Arava, Israel, *Tectonophysics,* **253,** 305–317.

Florensov, N.A. & Solonenko, V.P., 1963. *The Gobi Altay earthquake,* Akademiya Nauk USSR. Moscow.

Hanks, T.C., 1999. The age of scarplike landforms from diffusion-equation analysis, in *Quaternary geochronology,* pp. 313–338, ed. Stratton Noller J., Sowers, Lettis, AGU Washington DC.

Hanks, T.C. & Schwartz, D.P., 1987. Morphological dating of the pre-1983 fault scarp on the Lost River fault at Doublespring Pass Road, Custer County, Idaho, *Bull. seism. Soc. Am.,* **77,** 837–846.

Hanks, T.C., Bucknam, R.C., Lajoie, K.R. & Wallace, R.E., 1984. Modification of wave-cut and faulting-controlled landforms, *J. geophys. Res.,* **89,** 5771–5790.

Hanks, T.C., Ritz, J-F, Kendrick, K.J., Finkel, R.C. & Garvin, C.D., 1997. Uplift rates in a continental interior: faulting offsets of a ∼100 ka abandoned fan along the Bogd fault, southern Mongolia, *Proc. Penrose Conference on the Tectonics of Continental Interiors*.

Hirano, M., 1968. A mathematical model of slope developement—An approach to the analytical theory of erosional topography, *J. Geosci.,* **11,** 13–52.

Huc, M., Hassani, R. & Chery, J., 1998. Large earthquake nucleation associated with stress exchange between middle and upper crust, *Geophys. Res. Lett.,* **25,** 551–554.

King, G.C.P., Stein, R.S. & Rundle, J.B., 1988. The growth of geological structures by repeated earthquakes-1 Conceptual framework, *J. geophys. Res.,* **93,** 13,307–13,318.

Kurushin, R.A., Bayasgalan, A., Olziybat, M., Enhtuvshin, B., Molnar, P., Bayarsayhan, C., Hudnut, K. & Lin, J., 1997. *The surface rupture of the 1957 Gobi-Altay, Mongolia, earthquake,* Spec. Pap. Geol. Soc. Am., Vol. **320,** p. 143.

Leonard, G., Steinberg, D.M. & Rabinowitz, N., 1998. An indication of time-dependant seismic behaviour-an assessment of palaeoseismic evidence from the Arava fault, Israel, *Bull. seism. Soc. Am.,* **88,** 767–776.

Machette, M.N., 1987. Documentation of Benchmark photograph that show the effects of the 1983 Borah Peak earthquake with some considerations for studies of scarp degradation, *Bull. seism. Soc. Am.,* **77,** 771–783.

Mattson, A. & Bruhn, R.L., 1999. Comparison of linear and non-linear diffusion equation models as calibrated from shoreline scarps and multiple-event fault scarps: eastern Great Basin, *EOS Trans. Am. geophys. Un.,* **80,** 735.

McCalpin, P., 1996. *Palaeoseismology*, Academic Press Inc., New York.

Meghraoui, M., Philip, H., Albarède, F. & Cisternas, A., 1988. Trench investigations through the trace of the 1980 El Asnam thrust Fault: Evidence for Palaeoseismicity, *Bull. seism. Soc. Am.,* **78,** 979–999.

Molnar, P. *et al*., 1994. Quaternary Climate Change and the Formation of River Terraces across Growing Anticlines on the North Flank of the Tien Shan, China, *J. Geology,* **102,** 583–602.

Nash, D.B., 1981. FAULT: a Fortran programme for modeling the deradation of active normal fault scarps, *Computers and Geosciences,* **7,** 249–266.

Nash, D.B., 1984. Morphological dating of fluvial terrace scarps and fault scarps near West Yellowstone, Montana, *Geol. Soc. Am. Bulletin,* **95,** 1413–1424.

Nino, F., Philip, H. & Chery, J., 1998. The role of bed-parallel slip in the formation of blind thrust faults, *J. struct. Geol.,* **20,** 503–516.

Nivière, B., Marquis, G. & Maurin, J-C, 1998. Morphologic dating of slowly evolving scarp using a diffusive analogue, *Geophys. Res. Lett.,* **25,** 2325–2328.

Nivière, B. & Marquis, G., 2000. Evolution of terrave risers along the upper Rhine Graben inferred from morphologic dating methods: evidence of climatic and tectonic forcing, *Geophys. J. Int.,* **141,** 577–594.

Owen, L.A., Windley, B.F., Cunningham, W.D., Badamgarav, J. & Dorjnamjaa, D., 1997. Quaternary alluvial fans in the Gobi of southern Mongolia: evidence for neotectonics and climate change, *J. Quatern. Sci.,* **12,** 239–252.

Owen, L.A., Richards, B., Rhodes, E.J., Cunningham, W.D., Windley, B.F., Badamgarav, J. & Dorjnamjaa, D., 1998. Relic permafrost structures in the Gobi of Mongolia: age and significance, *J. Quatern. Sci.,* **13,** 539–547.

Owen, L.A., Cunningham, W.D., Richards, B.W.M., Rhodes, E.J., Windley, B.F., Dorjnamjaa, D. & Badamgarav, J., 1999. Timing of formation of forebergs in the northeastern Gobi Altai, Mongolia: implications for estimating mountain uplift rates and earthquake recurrence intervals, *J. Geol. Soc., Lond.,* **156,** 457–464.

Philip, H. & Megrhaoui, M., 1993. Structural analysis and interpretation of the surface deformations of the El Asnam earthquake of October 10, 1980, *Tectonics,* **2,** 17–49.

Philip, H., Rogozhin, E., Cisternas, A., Bousquet, J-C, Borisov, B. & Karakhanian, A., 1992. The Armenian earthquake of 1988 December 7: faulting and folding, neotectonics and palaeoseismicity, *Geophys. J. Int.,* **110,** 141–158.

Ritz, J-F, Brown, E.T., Bourlès, D.L., Philip, H., Schlupp, A., Raisbeck, G.M., Yiou, F. & Enkhtuvshin, B., 1995. Slip rates along active faults estimated with cosmic-ray-exposure dates: application to the Bogd fault, Gobi-Altai, Mongolia, *Geology,* **23,** 1019–1022.

Ritz, J-F *et al.*, 1999. Analysing the uplift rate along the Gurvan Bulag thrust fault (Gobi-Altay, Mongolia) during the upper Pleistocene, *EOS Trans. Am. geophys.Un,* **80,** 1039.

Roering, J.J., Kirchner, J.W. & Dietrich, W.E., 1999. Evidence for non-linear, diffusive sediment transport on hillslopes and implications for landscape morphology, *Wat. Resour. Res.,* **35,** 853–870.

Schwartz, D.P. *et al.*, 1996. Gobi-Altay, Mongolia, palaeoseismology expedition: initial results, *Eos Trans. Am.geophys. Un,* **78,** 462.

Siame, L. *et al*., 1997. Cosmogenic dating ranging from 20 to 700 ka of a series of alluvial fan surfaces by the El Tigre fault, Argentina, *Geology,* **25,** 975–978.

Stein, R.S., King, G.C.P. & Rundle, J.B., 1988. The growth of geological structures by repeated earthquakes—1 Field examples of continental dip-slip faults, *J. geophys. Res.,* **93,** 13 319–13 331.

Stirling, M.W., Wesnousky, S.G. & Shimazaki, K., 1996. Fault trace complexity, cumulative slip, and the shape of the magnitude-frequency distribution for strike-slip faults: a global survey, *Geophys. J. Int.,* **124,** 833–868.

Swan, F.H., 1988. Temporal clustering of palaeoseimsic events on the Oued Fodda fault, Algeria, *Geology,* **16,** 1092–1095.

Taboada, A., Bousquet, J-C & Philip, H., 1993. Coseismic elastic models of folds above blind thrusts in the Betic Cordilleras (Spain) and evaluation of seismic hazard, *Tectonophyisics,* **220,** 223–241.

Tapponnier, P. & Molnar, P., 1979. Active faulting and Cenozoic tectonics of the Tien Shan, Mongolian and Baykal regions, *J. geophys. Res.,* **84,** 3425–3459.

Wallace, R.E., 1977. Profiles and ages of young fault scarps, north-central Nevada, *GSA. Bull.,* **88,** 1267–1281.

Wesnousky, S.G., 1994. The Gutenberg-Richter or Characteristic Earthquake Distribution, Which Is It?, *GSA Bull.,* **84,** 1940–1959.

Yeats, R.S., Sieh, K.C. & Allen, R., 1997. The Geology of Earthquakes, Oxford University press, New York.

APPENDIX A: BEST FITTING MORPHOLOGICAL AGE AND UNCERTAINTY DETERMINATION

Fig. A1 illustrates two important points concerning the determination of the best fitting morphological age and its associated uncertainty: (1) best fitting morphological age does not depend on the assumed dip and location of faults if the distance between successive faults is large enough to preserve the morphology associated with each interseismic period. Conversely its associated uncertainty depends on the dip; (2) $\kappa\Delta t$ relative to the oldest events can not be determined with good accuracy independently of the other event. Thus, only a mean value of $\kappa\Delta t$ can be estimated from a cumulative scarp profile.

First, we want to evaluate how the morphological age depends on the fault dip assumption. We compute a profile using non-vertical stepping faults and we consider it as elevation data. We compare then the RMS versus $\kappa\Delta t$ when assuming true dip or vertical faults.

Fig. A1(a) shows the elevation profiles and the slope profiles of these two synthetic models. The first one ("reference profile") corresponds to a scarp formed by four successive surface ruptures caused by a stepping fault dipping 50° and three interseismic periods during which diffusion is applied after gravitational collapse at the front of the scarp. The last event has not been followed by the interseismic period, so that the gravity-controlled face is preserved at the front of the scarp. The distance between faults allows us to identify several inflections of the slope profile corresponding to the successive surface ruptures. The second profile ("adjusted profile") fits with the previous one, assuming that successive faults are vertical. The fitting of this profile is based on the analysis of the slope profile of the reference profile, as we do when we want to model real data. Fig. A1(b) shows the RMS versus constant $\kappa\Delta t$ obtain for both assumptions

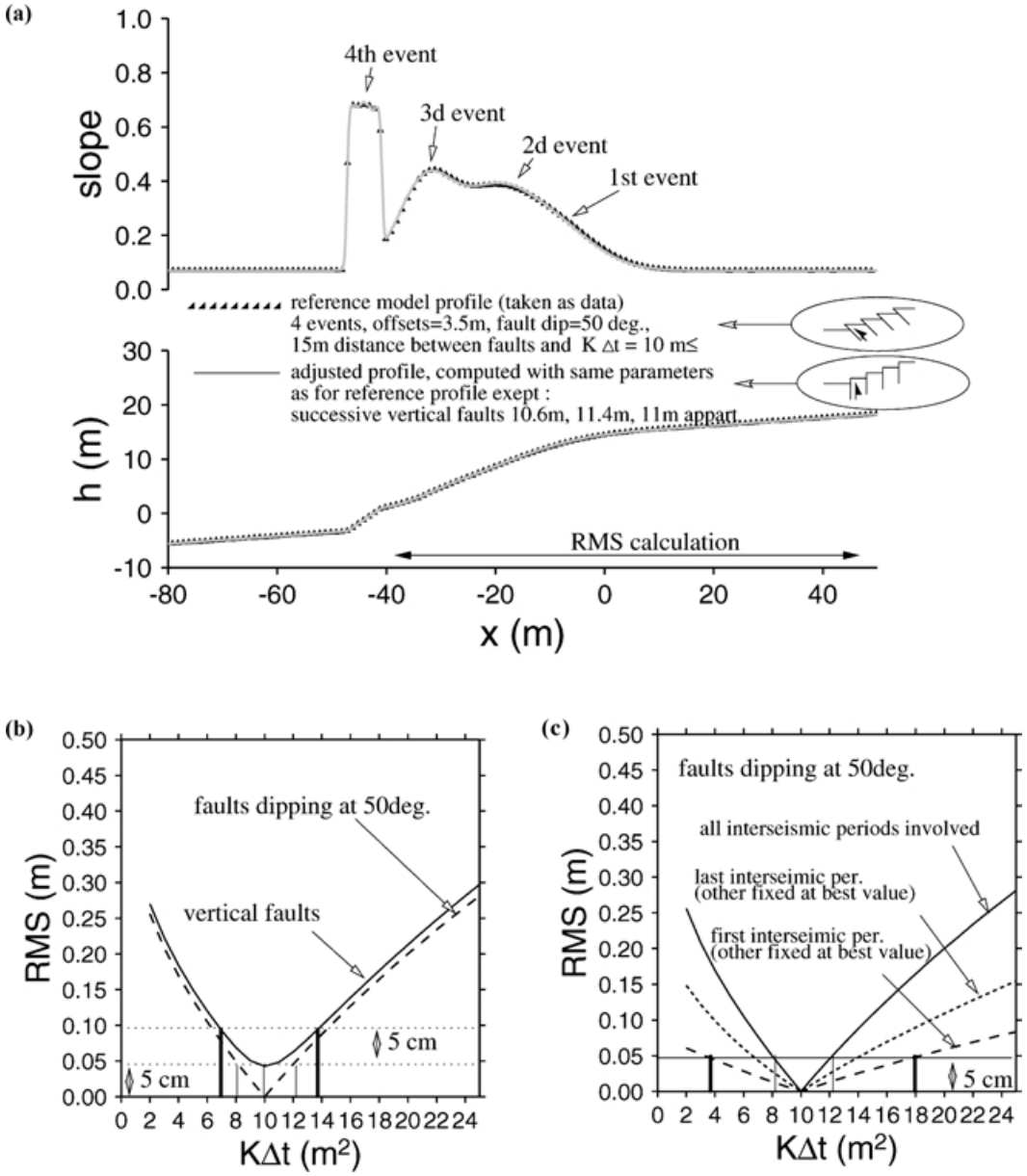

Figure A1. Best fitting morphological age and uncertainty determination. a) slope profile and elevation profiles for two models differing by the dip of faults. Both models use four successive stepping faults and 3.5 offsets. The reference profile uses faults dipping at 50°, while the adjusted profile uses vertical faults. To obtain this profile, we adjusted the location of the vertical faults so that inflections of its slope profile corresponds with those of the reference slope profile, as we would do when modelling real data. b) RMS versus constant $\kappa\Delta t$ when assuming true dip of faults (50°) or incorrect vertical faults. Reference profile is sampled at constant intervals and taken as data. The horizontal dotted lines correspond to the RMSmin +5 cm limits beneath which we consider that models are acceptable. Both RMS curves have a minimum value at $\kappa\Delta t = 10$ m^2. However, the uncertainty of the best fitting value of $\kappa\Delta t$ is larger when assuming incorrect vertical faults. This shows that fault dip does not affect the determination of the best fitting $\kappa\Delta t$ when morphology is preserved from collapse, but it affects the precision of the estimate. c) RMS versus constant $\kappa\Delta t$ when assuming true dip of faults (50°). Reference profile is taken as data. The different RMS curves were obtained using either all interseismic durations as free parameters, or only one of them. In the second case, the other interseismic durations are fixed at the best fitting value ($\kappa\Delta t = 10$ m^2). The horizontal line corresponds to the RMSmin +5 cm limit beneath which we consider that models are acceptable. It shows that uncertainty grows when the parameter search procedure is applied to only one interseismic duration. In particular, the value of $\kappa\Delta t$ is poorly resolved for the first (older) interseismic duration.

(vertical and non-vertical faults). Computation of RMS is restricted to the portion of the scarp located back to the gravity-controlled face (for which the slope has no meaning in terms of morphological age). In order to obtain the RMS curve corresponding to the faults dipping at 50° (dashed line) we sampled the corresponding elevation profile ("reference profile") at specified intervals and we incremented $\kappa\Delta t$. The resulting RMS curve has a zero value at the expected best fitting value $\kappa\Delta t = 10$ m^2. The second curve (solid line) corresponds to RMS values computed from "reference profile" assuming vertical faults. This RMS curve has also a minimum value at the best fitting $\kappa\Delta t = 10$ m^2. We define confidence intervals on the best fitting value of $\kappa\Delta t$ by considering all profiles that fit data within 5 cm of minimum RMS (see horizontal lines in Fig. A1b). While best fitting $\kappa\Delta t$ does not depend on the assumed dip of faults, Fig. A1(b) shows that this interval is clearly greater when assuming incorrect dip. As far as reverse faults are usually not vertical, it is reasonable to assume arbitrary dipping faults to reduce the uncertainty on best fitting value. The foregoing illustrates the need to improve the determination of morphological ages on cumulative scarps by a more general parameter search, including dip and location of the faults.

Fig. A1(c) deals with the accuracy expected when determining the value of $\kappa\Delta t$ for old events. We have computed RMS curves from the reference profile, assuming correct dip of faults (50°). We have incremented the value of $\kappa\Delta t$ for all events (solid line), or only one of them (dashed and dotted lines). In the last case, the other values of $\kappa\Delta t$ are fixed at the best fitting value. The horizontal line corresponds to the value of minimum RMS plus 5 cm which allows to determine confidence intervals on the best fitting values. As expected, RMS curves have a zero value at the best fitting value. However, the confidence intervals are larger when varying a single $\kappa\Delta t$. The accuracy of the estimate becomes poor if we want to estimate the value of $\kappa\Delta t$ associated with the oldest event (dashed line, Fig. A1c). This implies that it is not possible to estimate each interseismic duration with a good accuracy. On the contrary, a mean value of $\kappa\Delta t$ can be determined, which leads to a mean value of the morphological age of a cumulative scarp by multiplying this value by the number of interseismic periods.